Ref: FOI2021-014

███████████████

15th November 2021

Dear ███████

Further to our email of 8th October 2021 regarding your request for the following information:

> *I formally request under the Freedom of Information Act, documents relating to the human experimentation of Nuclear materials as referenced by the attached report.*
>
> *Specifically, my request should include the following scope:*
>
> *- Between 1957 and 1987 injecting strontium-85 on a number of occasions into the same human subject*
>
> *- in the 1960s, the inhalation of radioactive iodine isotopes*
>
> *- from 1972 to 1976, three male British subjects inhaled palladium-103 ('mock' plutonium) and chromium-51*
>
> *- From 1979 to 1985, 19 British men and women inhaled niobium-92m (another 'mock' plutonium)*
>
> *- From 1986 to 1988, two British volunteers were injected with barium-133. One of the two was also injected with strontium-85.*
>
> *- From 1988 to 1990 eight male British volunteers - including five who had previously inhaled niobium - took part in a repeat study.*
>
> *These experiments were referenced by President Bill Clinton in the Human Experimentation inquiry carried out by the US givernment.*

Your request has been handled as a request for information under the Freedom of Information Act 2000 (the Act).

We can confirm that the Atomic Weapons Establishment (AWE) holds some information in scope of your request. We will address each part of your request individually:

Between 1957 and 1987 injecting strontium-85 on a number of occasions into the same human subject

No information is held by AWE.

In the 1960s, the inhalation of radioactive iodine isotopes

AWE is the trading name of AWE plc. AWE is a Non-Departmental Public Body owned by the Ministry of Defence. Registered in England and Wales. Registration no. 02763902. Registered office: Room 20, F161.2, AWE plc, Aldermaston, Reading, Berkshire RG7 4PR

UK Ministry of Defence © Crown Owned Copyright 2021/AWE

No information is held by AWE.

<u>From 1972 to 1976, three male British subjects inhaled palladium-103 ('mock' plutonium) and chromium-51</u>

We can confirm AWE holds information related to this part of your request, a report entitled *'Harwell Report 1983 – Validity of the Livermore Phantom for Male Subjects'*.

This report originated from Harwell which now comes under the umbrella of the Nuclear Decommissioning Authority, and includes data provided by US laboratories.

For this reason, we considered withholding the report under section 27 of the Act, which states that information is exempt if it is confidential information obtained from a State other than the United Kingdom or from an international organisation or international court. This exemption is a qualified exemption and is subject to a Public Interest Test (PIT), consequently a PIT was carried out.

The main argument in favour of withholding the information is that the report is a preliminary study and at the time it was written there were discrepancies which were yet to be resolved. It isn't clear from the draft if the United Kingdom and the United States resolved those differences. AWE was concerned that releasing it may damage the relationship between AWE and those Laboratories.

However, on consultation with the Nuclear Decommissioning Agency (NDA) it has been determined that the document appears to be a draft of a later published unclassified document with very little change. As a great deal of the US lab's data in the report is already in the public domain and the FOI Act contains a presumption in favour of disclosure, and as AWE wishes to promote openness and transparency, on balance AWE have determined that the public interest lies in the document being released. Therefore, please see the attached Harwell Report 1983.

Certain parts of the document have been redacted where the information is exempt from disclosure under section 40(2) of the Act. This exempts personal data if disclosure would breach any of the data protection principles. This is an absolute exemption and is not subject to the PIT.

<u>From 1979 to 1985, 19 British men and women inhaled niobium-92m (another 'mock' plutonium)</u>

We can confirm AWE holds information related to this part of your request, please see attached: *O Report 24/87 – Investigation of the Distribution of Activity in the Lungs and its Effect on the In-Vivo Measurement of Am-241* and *O Report 7/86 – Calibration of X-ray Counters for Assessment of Internal Lung Contamination, with Low Energy X-ray Emitters, in Women Part 1: Measurements Made at AWRE Aldermaston.*

The attached Harwell Report 1983 (mentioned above) also contains information in scope.

Certain parts of these documents have been redacted where the information is exempt from disclosure under section 40(2) of the Act. This exempts personal data if disclosure would breach any of the data protection principles. This is an absolute exemption and is not subject to the PIT.

Also in scope of your request are two papers entitled *Improved Counting Efficiencies For Measuring 239Pu in the Lung in the Sitting Position (Palmer et al., 1989)* and *The Livermore Phantom as a Calibration Standard in the Assessment of Plutonium in Lungs (Newton et al., 1984).*

However, these documents fall entirely within the exemption provided for under section 21 of the Act (Information accessible to applicant by other means).

The Palmer et al. (1989) paper was published in Health Physics: November 1989 - Volume 57 - Issue 5 - p 747-752 and can be bought here: https://journals.lww.com/health-physics/Abstract/1989/11000/Improved_Counting_Efficiencies_for_Measuring_239Pu.7.aspx

The Newton et al. (1984) paper can be found here: http://citeseerx.ist.psu.edu/viewdoc/download?doi=10.1.1.880.2353&rep=rep1&type=pdf#page=197

From 1986 to 1988, two British volunteers were injected with barium-133. One of the two was also injected with strontium-85.

No information is held by AWE.

From 1988 to 1990 eight male British volunteers - including five who had previously inhaled niobium - took part in a repeat study.

No information is held by AWE.

Please remember to quote the reference number above in any future communications. If you have any queries regarding the content of this letter, please contact this office in the first instance.

If you are unhappy with the way your request has been handled you have a right to request an internal review within 40 days of receiving this letter, by writing to information.requests@awe.co.uk or our postal address: Information Requests Team, AWE Aldermaston, Reading, RG7 4PR. If you are still unhappy after an internal review has been completed, under the provisions of Section 50 of the Freedom of Information Act 2000 you have the right to take your complaint to the Information Commissioner's Office. Please note the Commissioner will generally not consider a complaint until you have exhausted AWE's internal complaints process.

Yours sincerely,

AWE Information Requests Team

VALIDITY OF THE LIVERMORE PHANTOM FOR MALE SUBJECTS

During the past four years, Harwell has been collaboratoring with several other laboratories in an assessment of the validity of the phantom as a calibration standard for low energy X ray emitters. The experimental subjects were eight volunteers who inhaled 5-μm polystyrene particles labelled with ^{92m}Nb, emitting 15.8-17.7-keV X rays and 934-keV gamma rays. The gamma ray emissions allow the radioactive content of the lungs to be determined as a function of time after intake, independently of X-ray counting, so that the subject can be used to calibrate X-ray counters, and the derived calibration factor can be compared with that indicated by the phantom, with ^{92m}Nb-labelled lungs, for his particular physique.

The attached tables (1-10) and graphs (numbered 3,6,7,9 and 11) are extracted from a report to our sponsors (IAEA), currently in preparation. They should not be made available to anyone outside your own organisation. There are two reasons why this would be improper: (i) our sponsors have not yet received these details, and (ii) much of the information is based on material provided by collaborating laboratories, which have not yet received copies for comment and confirmation that I have interpreted their data correctly. References to "Figures" in the tables should be ignored; the only illustrations provided here are the above-mentioned graphs.

Table 1   summarises the relevant physical data of three relevant nuclides: ^{239}Pu, ^{92m}Nb and ^{103}Pd. ^{103}Pd was previously employed in work of this general nature, but, compared with those from Pu, its X rays are attenuated some 4-5 times less effectively in subjects of typical physique and its use for the present purposes was felt to provide an insufficiently stringent test of the phantom's validity. The X rays from ^{92m}Nb are typically attenuated 1.5 times more severely than those from Pu.

Table 2   indicates the methods used by participating laboratories to assess the subjects' gamma-ray emissions in lungs, as a basis for determining the associated X-ray emissions, and also the X ray counters for which calibration data were sought.

Table 3   contains personal details of the subjects and the results of
           gamma-ray counting. The data from ANL (by counting in distant
           arc geometry), coupled with the effective half-lives listed,
           were used to calculate the associated X-ray emissions in the
           lungs, as a function of time after intake. Graph 3 shows the
           ^{92m}Nb content, by gamma-ray counting, of one subject. The
           effective half-life (9.2 days), coupled with the half life of
           10.16 days by radioactive decay, implies a half-life of 97 days
           for the clearance of the particles.

Table 4   gives data on chest wall thickness and composition. The CWTs
           from AWRE and PNL are consistent, those from LLNL are invariably
           higher. The discrepancy has not been resolved. Both LLNL and
           AWRE point to CWT measurements independent of ultrasonics, which
           each suggests validates its own assessments. We have adopted,
           as our best estimate, the mean of the three laboratories'
           estimates, while however showing, in subsequent tables, the
           effect on our conclusions if the lower estimates from AWRE and
           PNL were held to be correct. Only AWRE and LLNL measured
           adipose tissue thicknesses, and here they generally agreed.

Table 5   may not be particularly useful in the absence of explanatory
           material not provided here. It gives the rate at which the X-
           ray count declined as overlayers of various types were added to
           the basic phantom, with lungs labelled with ^{92m}Nb.

Table 6   shows observed (i.e. in our subjects) and predicted (i.e. from
           the phantom) X-ray detection efficiencies for the small phoswich
           detectors (Table 2) used at LLNL and at PNL. To get the
           predicted values, each subject's "Equivalent Muscle Thickness"
           (EMT) was first calculated. This is simply the thickness of
           muscle-equivalent material providing the same attenuation as the
           combination of actual thicknesses of muscle and adipose tissue
           present in the subject. EMT is a function of these latter
           thicknesses and of the relevant half-value thicknesses for
           muscle-equivalent and adipose-equivalent materials given in

2

Table 5. The calibration function with muscle-equivalent layers (Graph 6), evaluated for the appropriate EMT, then gives the predicted efficiency for the subject. The agreement between observed and predicted efficiencies may be judged from the ratios in Table 6 or from Graph 6, where the observed efficiencies are also plotted.

Table 7 and Graph 7

show the same data for paired 8" dia. phoswich detectors (Table 2) at Harwell and at ANL.

Table 8   gives the same data for a single, centrally-placed phoswich detector at Harwell and at ANL. There are differences here, ANL's results suggesting that the phantom is valid on average, Harwell's suggesting that it is not.

Table 9 and Graph 9

show results for LLNL's paired square phoswich detectors, available for measurements on six subjects only.

Table 10   gives a summary of the data from Tables 6-9. For paired detectors (overall mean efficiency ratio 0.98) the phantom appears generally to be valid, and this conclusion is not drastically affected (ratio 0.84) if the lower CWT values from AWRE and PNL are preferred to the three-lab means. The variability of individual means (range 0.82-1.19) contributing to the grand mean (0.98), even with detectors of identical or similar size, is likely to reflect small differences in positioning criteria, coupled with observations (see below) that the pattern of flux distribution over the surface of the phantom's chest was not wholly typical of that in our subjects. In this situation there would seem to be advantages, in terms of calibration if not sensitivity, in having complete coverage of the frontal surfaces of the upper thorax. In the system (LLNL's square phoswiches) in which this coverage was most nearly complete, the standard deviation (± 0.11) of efficiency ratios in the subjects was the lowest for all systems. Discrepancies

3

between Harwell's and ANL's data for a single phoswich presumably also reflect differences in positioning criteria, although none has been identified.

Graph 11   shows the results of attempts to derive efficiencies for Pu in lungs from Harwell's data for ^{92m}Nb and for ^{103}Pd, by adjusting for differential attenuation. The data plotted at EMT = 17.7 mm are for the same subject, who participated in experiments with both nuclides, and their agreement shows that adjustments for differential attenuation can work. The prediction from the phantom, with ^{238}Pu-labelled lungs, is also shown; these latter efficiencies are genuine X-ray detection efficiencies, the scatter component from emissions of higher energy having been subtracted.

Additional comments   (not supported by detailed data in this summary).

The distribution of X ray flux over the surface of the phantom's thorax was not typical. The usual lateral asymmetry (more from the right side) was more marked in the case of the phantom. Other differences emerged from studies at ANL and at AWRE.

EMSc Division
AERE Harwell

1st December 1983

4

TABLE 1

X-RAY EMISSIONS FROM ^{103}Pd, ^{239}Pu AND ^{92m}Nb AND THEIR ATTENUATION IN SOFT TISSUES

NUCLIDE	X-RAY SERIES	ENERGY (keV)	ABUNDANCE (%)	LINEAR ATTENUATION COEFFICIENT*, cm^{-1}	
				MUSCLE	ADIPOSE TISSUE
^{103}Pd [†]	Rh K$_\alpha$	20.2	67	0.69	0.43
	K$_\beta$	22.8	13	0.53	0.34
^{239}Pu [†]	U L$_\alpha$	13.6	1.67	1.98	1.07
	L$_\beta$	17.2	2.38	1.02	0.60
	L$_\gamma$	20.2	0.55	0.69	0.43
^{92m}Nb [‡]	Zr K$_\alpha$	15.8	53.6	1.29	0.73
	K$_\beta$	17.7	9.9	0.95	0.56

* Sum of coefficients for photoelectric absorption and Compton scattering, based on calculations by ████████ using methods given in ref 19. Elemental compositions were assumed, from refs 20 (muscle) and 21 (adipose tissue).

† X-ray abundances estimated as described in ref 17.

‡ X-ray abundances as given in ref 9.

TABLE 2 EQUIPMENT AND TECHNIQUES USED TO STUDY SUBJECTS' GAMMA- AND X-RAY EMISSIONS

LABORATORY	ASSESSMENTS OF GAMMA-RAY EMISSIONS IN LUNGS AND/OR EFFECTIVE HALF-LIFE OF ^{92m}Nb IN LUNGS	INVESTIGATIONS OF X-RAY EMISSIONS
HARWELL	NaI(Tl) crystal, 230 mm-dia. x 150 mm, (i) viewing anterior surfaces of supine thorax and (ii) viewing posterior surfaces, at 230 mm distance in both cases. Combined response compared with that from a phantom with ^{92m}Nb distributed in lungs, with allowance for estimated differential attenuation.	200 mm-dia. (190 mm effective[x]) phoswich viewing frontal surfaces of supine thorax. Geometry 1: detector central over mid-sternum Geometry 2: combined response of detector viewing left and right lungs sequentially
ANL	NaI(Tl) crystal, 152 mm-dia. x 203 mm, in 1.5 m arc geometry. Subject measured prone and supine. Calibration factor estimated from response to a standardised point source of ^{92m}Nb with allowances for differences in geometry and attenuation[12].	200 mm-dia. phoswich as at Harwell (both geometries). Also, 180 mm-dia. Xe/CH$_4$ proportional counter with 50 mm x 50 mm hole collimator, used to study pattern of emission over frontal surface of thorax.
LLNL	NaI(Tl) crystal, 290 mm-dia. x 102 mm, placed 445 mm above horizontal mid-plane of supine thorax.	(i) Paired 114 mm-dia. phoswich detectors, one viewing each lung, positioned with sternum and clavicle tangential to periphery of detector; (ii) paired 152 x 152 mm^2 square detectors giving essentially complete coverage of anterior surface between sternal notch and ziphoid process[22].
PNL	NaI(Tl) crystal, 238 mm-dia. x 102 mm. Sequential measurements with anterior and posterior surfaces at 1.0 m from detector.	Paired 127 mm-dia. phoswich detectors, located as for LLNL (i).
AWRE		Arrays of 44 mm-dia. (effective) high-purity Ge detectors. Six detectors viewing each lung (Fig 2).

x apparent diameter from scanning window with a collimated X-ray source (full width at half maximum response).

TABLE 3

DETAILS OF EXPERIMENTAL SUBJECTS AND THEIR PULMONARY RETENTION OF ^{92m}Nb
Data on chest wall thickness and composition are given in Table 4

SUBJECT	WEIGHT (kg)	HEIGHT (m)	AGE (yr)	IPD (kBq)[*]		EFFECTIVE HALF-LIFE IN LUNGS T_E		
				ANL estimate	HARWELL estimate	T_E (days)	Measured by (lab)	Observation period (days post-intake)
				15.9	16.4	9.72±0.03	HARWELL	3 - 94
				19.0	18.8	9.52±0.04	HARWELL	4 - 54
				168	170	9.97±0.05	ANL	12 - 123
				55.1	54.6	9.92	LLNL	4 - 117
				15.8	14.5	9.76±0.04	HARWELL	3 - 29
				34.8	30.6	9.70±0.02	HARWELL	5 - 49
				—	25.5			
				18.7[†]	—	9.41	LLNL	22 - 90
				50.9	49.9	9.20±0.03	HARWELL	4 - 50

[*] Initial pulmonary deposit, ie deposit in regions of lung from which clearance is slow, with the effective half-lives T_E given.

[†] At time of supplementary intake 8 days after the first; see text.

^{92m}Nb in lungs, kBq

Days after intake

$49.9 \exp \left\{ \dfrac{-0.693}{9.2} t \right\}$

○ AERE
△ ANL

3
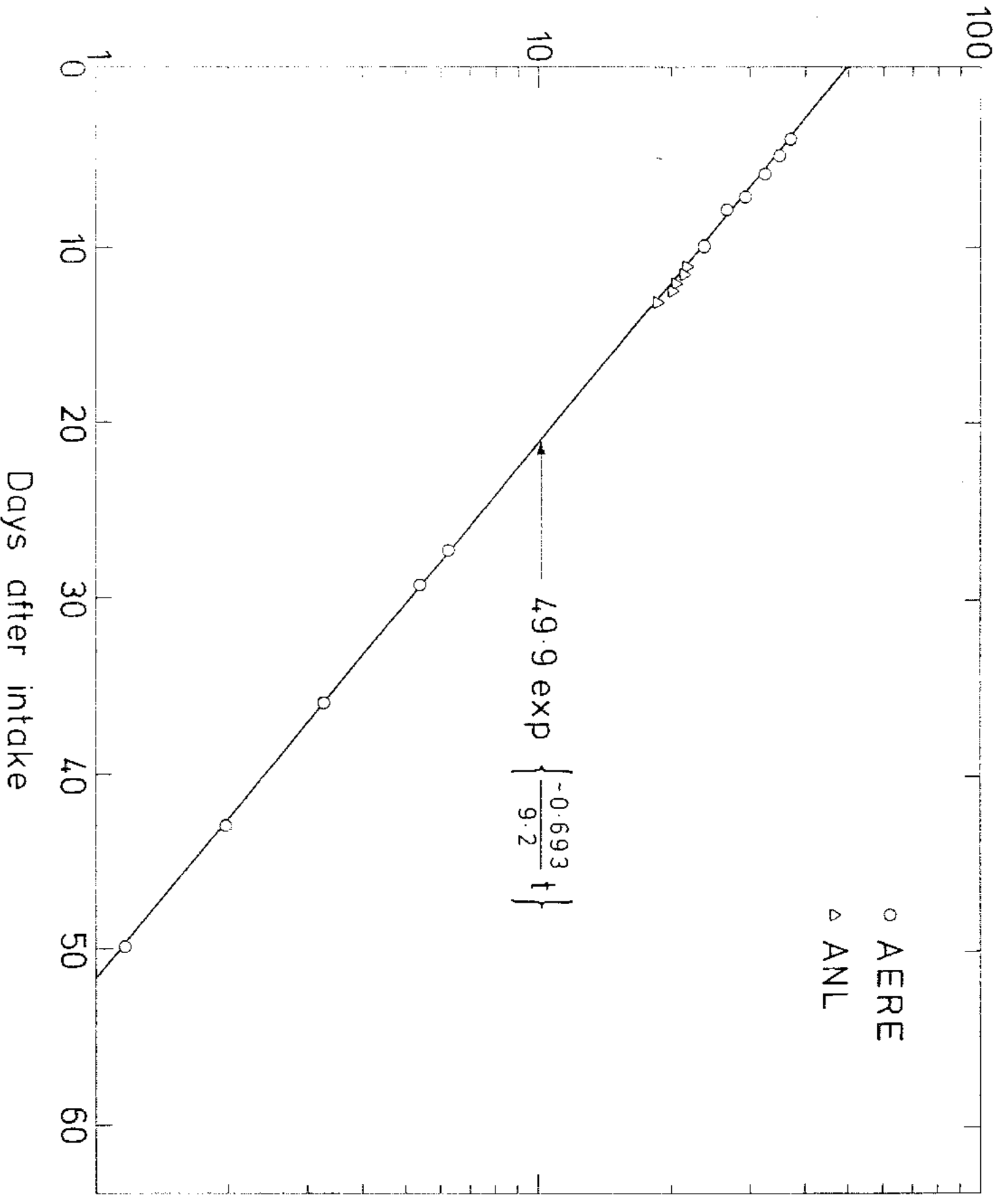
TABLE 4   ESTIMATES OF CHEST WALL THICKNESS AND COMPOSITION

SUBJECT	CHEST WALL THICKNESS (mm)				PERCENTAGE OF ADIPOSE TISSUE		
	AWRE	PNL	LLNL	Mean (3 labs)	AWRE	LLNL	Mean (2 labs)
███████	19.1	18.8	21.4	19.8	25	28	26.5
	29.1	28.7	32.1	30.0	33	32	32.5
	29.7*	29.0	34.4	31.0*		43	(43)
	27.6	28	28.9	28.2	30	32	31
	20.8	19	24.3	21.4	33	31	32
	20.6	20.7	24.9	22.1	30	32	31
	31.8	33.4	37.0	34.1	30	38	34
	26.7	26.2	30.5	27.8	32	31	30.5
MEAN (8 subjects)	25.7	25.5	29.2	26.8			

* AWRE did not measure CWT in Subject ███ the values given were inferred from his CWT measured
  at PNL and LLNL, and mean relationships between laboratories' estimates for other subjects.

† Values of CWT for Subject ███ are higher than previously reported (1,4,5). See Appendix for
  an explanation.

TABLE 5   REDUCTION IN RESPONSE FROM PHANTOM WITH INCREASING THICKNESS OF OVERLAYER

Data are Half-Value Thicknesses (HVT), ie thicknesses (mm) necessary to reduce
X-ray count rate by a factor of two. Values in parentheses are calculated from
the observed values for MEM and 87A layers, according to Equations 3 or 4

OVERLAYER MATERIAL equivalent to	2 SMALL DETECTORS[*]		2 x 150-mm SQUARE DETECTORS	2 x 200-mm-dia. DETECTORS (GEOMETRY 2)		SINGLE 200-mm-dia. DETECTOR (GEOMETRY 1)	
	LLNL	PNL	LLNL	HARWELL	ANL	HARWELL	ANL
MUSCLE (MEM)	4.4	4.4	5.4	4.8±0.4	4.5±0.2	4.5±0.4	4.5±0.2
87% ADIPOSE + 13% MUSCLE (87A)	7.0	7.8		6.9±0.2	7.7±0.4	6.6±0.2	8.0±0.5
50% ADIPOSE + 50% MUSCLE (50A)	(5.6)	6.0(5.9)		5.9(5.8)		5.5(5.5)	
ADIPOSE TISSUE (AEM)	(7.7)	(8.8)		(7.4)	(8.6)	(7.1)	(9.2)

[*] 114 mm dia. (LLNL), 127 mm dia. (PNL)

TABLE 6   X—RAY DETECTION EFFICIENCIES E_{Nb} (counts per 10^4 Zr K X rays emitted in lungs) FOR SMALL PAIRED PHOSWICH DETECTORS AT LLNL AND AT PNL

SUBJECT		L L N L				P N L		
	EMT[*] (mm)	OBSERVED E_{Nb}[†]	PREDICTED E_{Nb}[‡]	RATIO Obs/Pred	EMT[*] (mm)	OBSERVED E_{Nb}[†]	PREDICTED E_{Nb}[‡]	RATIO Obs/Pred
	17.6	5.8±0.8 (4)	7.8	0.74	17.2	5.7±1.7 (6)	10.4	0.55
	25.8	1.8±0.4 (7)	2.1	0.86	25.1	1.8±0.2 (2)	3.0	0.60
	25.3	1.9±0.2 (5)	2.3	0.83	24.3	2.3±0.3 (3)	3.4	0.68
	24.5	2.8±0.2 (4)	2.6	1.08	23.8	3.4±0.2 (3)	3.6	0.94
	18.5	6.7±0.7 (4)	6.8	0.99	18.0	7.4±0.5 (4)	9.1	0.81
	19.2	5.7±0.2 (4)	6.1	0.93	18.7	5.8±0.4 (5)	8.2	0.71
	29.1	1.6±0.1 (5)	1.3	1.23	28.3	2.1±0.3 (5)	1.8	1.17
	24.2	3.8±0.5 (6)	2.8	1.36	23.6	4.2±0.3 (4)	3.8	1.11
MEAN ± sd				1.00±0.21 (0.85±0.18)[**]				0.82±0.23 (0.70±0.19)[**]

[*]   Equivalent muscle thickness (Equation 5)
[†]   Means and standard deviations, with number of observations in parentheses
[‡]   From Equation 6 (LLNL) or Equation 7 (PNL)
[**] Mean ratio if subjects' mean CWT values from AWRE and PNL (Table 4) are preferred to the higher three-laboratory means (paragraph 28)

PNL

LLNL

PHANTOM + MUSCLE LAYERS

6

EQUIVALENT MUSCLE THICKNESS ᴍᴍ
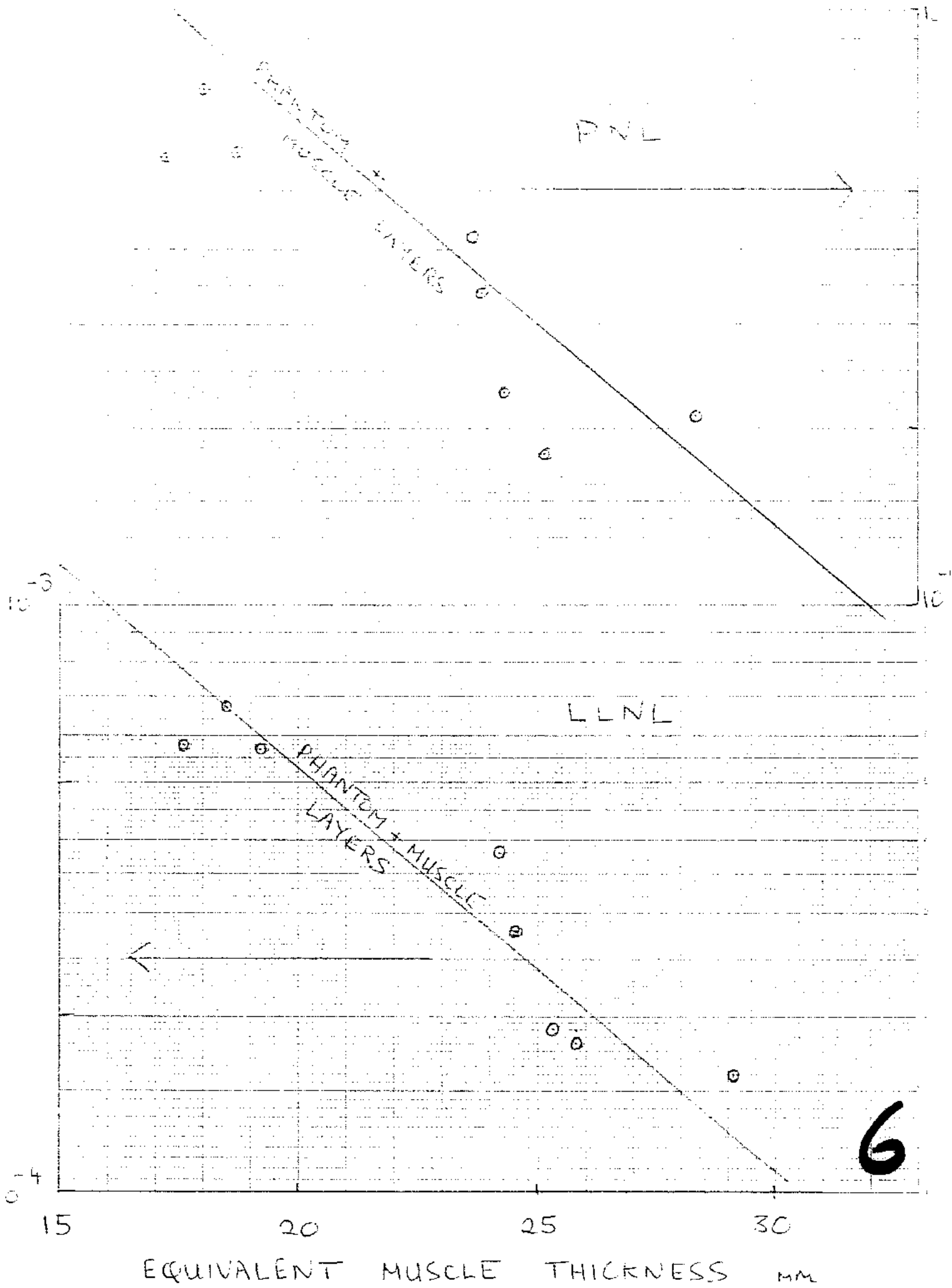
TABLE 7   X-RAY DETECTION EFFICIENCIES E_{Nb} (counts per 10^4 Zr K X rays emitted in lungs) FOR PAIRED 200-mm-DIA. PHOSWICH DETECTORS, IN GEOMETRY 2 AT HARWELL AND ANL

SUBJECT		HARWELL				ANL		
	EMT[*] (mm)	OBSERVED E_{Nb}[†]	PREDICTED E_{Nb}[‡]	RATIO Obs/Pred	EMT[*] (mm)	OBSERVED E_{Nb}[†]	PREDICTED E_{Nb}[‡]	RATIO Obs/Pred
	18.0	10.8±1.4 (8)	7.7	1.40	17.3	12.8 (1)	10.7	1.20
	26.6	2.8±0.4 (7)	2.2	1.27	25.4	1.7 (1)	3.1	0.55
	26.3	3.0±0.3 (5)	2.3	1.30	24.6	3.1 (2)	3.5	0.89
	25.1	2.7±0.2 (7)	2.7	1.00	24.0	3.8 (2)	3.8	1.00
	19.0	6.6±0.8 (15)	6.6	1.00	18.1	7.6 (1)	9.4	0.81
	19.7	6.8±0.5 (9)	6.0	1.13	18.8	7.3±0.4 (4)	8.5	0.86
	30.0	2.0±0.2 (12)	1.4	1.43	28.6	2.1±0.02 (3)	1.9	1.11
	24.8	2.9±0.3 (11)	2.9	1.00	23.8	3.8±0.5 (4)	4.0	0.95
MEAN ± sd				1.19±0.18 (1.02±0.16)[**]				0.92±0.20 (0.79±0.19)[**]

[*] Equivalent muscle thickness (Equation 5)
[†] Means and standard deviations, with number of observations in parentheses
[‡] From Equation 8 (Harwell) or Equation 9 (ANL)
[**] Mean ratio if subjects' mean CWT values from AWRE and PNL (Table 4) are preferred to the higher three-laboratory means (paragraph 28)

PHANTOM + MUSCLE LAYERS

HARWELL

7

EQUIVALENT MUSCLE THICKNESS cm
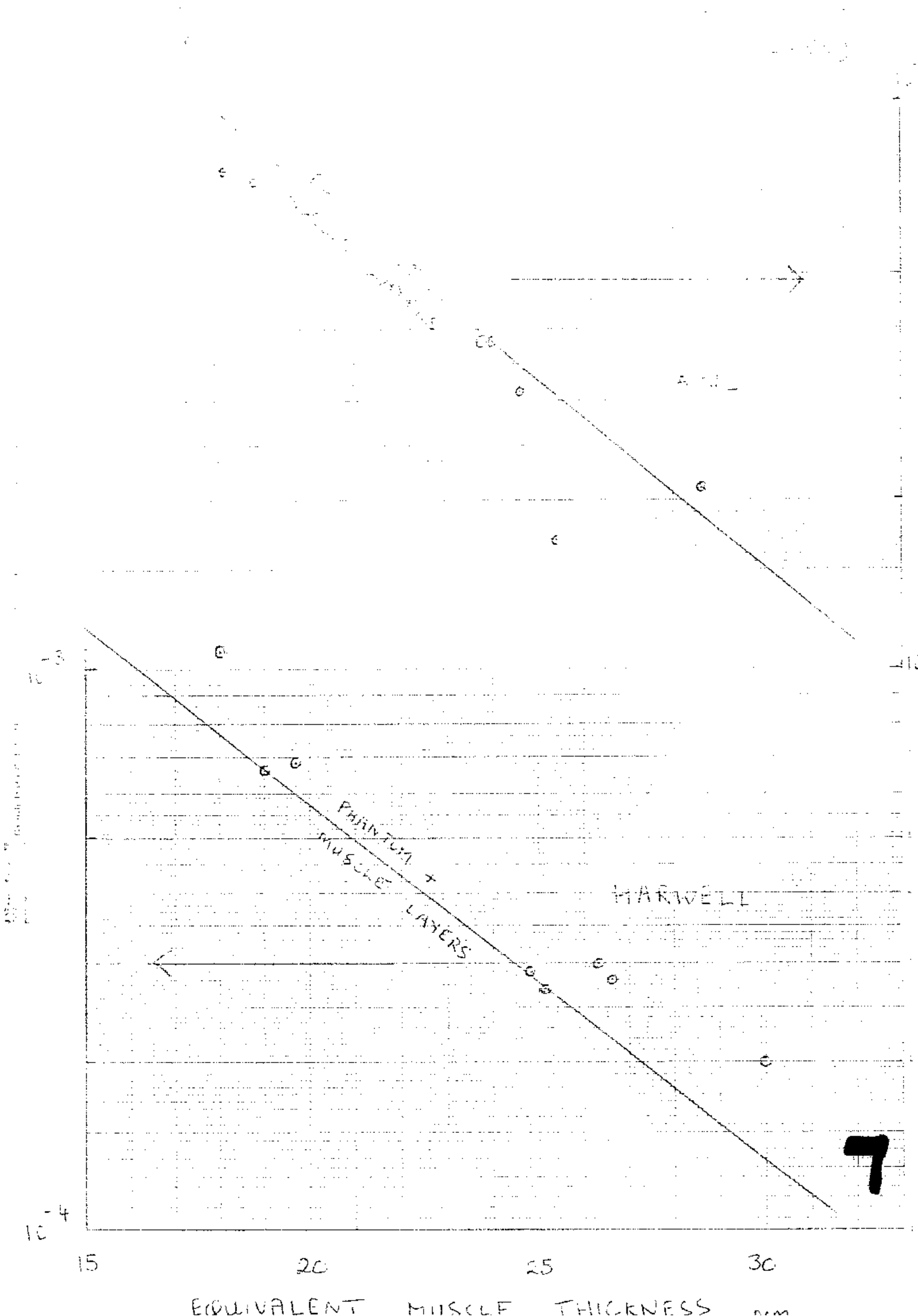
TABLE 8   X–RAY DETECTION EFFICIENCIES E_{Nb} (counts per 10^4 Zr K X rays emitted in lungs)
FOR A SINGLE, CENTRAL 200-mm-DIA. PHOSWICH DETECTOR (GEOMETRY 1 AT HARWELL AND AT ANL)

SUBJECT	HARWELL				ANL			
	EMT* (mm)	OBSERVED E_{Nb}[†]	PREDICTED E_{Nb}[‡]	RATIO Obs/Pred	EMT* (mm)	OBSERVED E_{Nb}[†]	PREDICTED E_{Nb}[‡]	RATIO Obs/Pred
	17.9	6.8±1.1 (9)	4.5	1.51	17.0	5.3±0.3 (8)	7.3	0.73
	26.4	2.3±0.6 (7)	1.2	1.92	24.8	2.2 (2)	2.1	1.05
	26.1	2.0±0.1 (5)	1.3	1.54	23.9	2.2±0.2 (5)	2.4	0.92
	25.0	2.2±0.2 (6)	1.5	1.47	23.5	2.1±0.5 (11)	2.5	0.84
	18.9	6.1±0.7 (17)	3.8	1.60	17.8	5.9±1.0 (8)	6.5	0.91
	19.6	4.8±0.6 (11)	3.4	1.41	18.5	5.5±0.5 (5)	5.8	0.95
	29.9	1.7±0.3 (12)	0.71	2.39	27.9	2.4±0.5 (4)	1.3	1.85
	24.7	3.0±0.3 (11)	1.6	1.88	23.3	3.9±0.7 (9)	2.7	1.44
MEAN ± sd				1.72±0.33 (1.46±0.25)**				1.09±0.37 (0.93±0.32)**

*   Equivalent muscle thickness (Equation 5)

†   Means and standard deviations, with number of observations in parentheses

‡   From Equation 10 (Harwell) or Equation 11 (ANL)

**   Mean ratio if subjects' mean CWT values from AWRE and PNL (Table 4) are preferred to the higher three-laboratory means (paragraph 28)

TABLE 9   X-RAY DETECTION EFFICIENCIES E_{Nb} (counts per 10^4 Zr K X rays emitted in lungs)
FOR PAIRED 150-mm-SQUARE PHOSWICH DETECTORS AT LLNL

SUBJECT	EMT, mm[*]	OBSERVED[‡] E_{Nb}	PREDICTED[†] E_{Nb}	RATIO Obs/Pred
	25.1	4.2 (2)	4.4	0.95
	24.3	4.7 (1)	4.8	0.98
	18.4	9.9 (1)	10.3	0.96
	19.1	7.8 (2)	9.4	0.83
	29.0	2.9 (2)	2.6	1.12
	24.1	5.6 (3)	5.0	1.12
MEAN ± sd				0.99±0.11 (0.84±0.10)[**]

[*]   Equivalent muscle thickness; mean of values appearing in Tables 6 and 7
[‡]   The number of observations is given in parentheses; where two or more, the value is the mean
[†]   From Equation 12
[**] Mean ratio if subjects' mean CWT values from AWRE and PNL (Table 4) are preferred to the higher three-laboratory means (paragraph 28)

EQUIVALENT MUSCLE THICKNESS MM
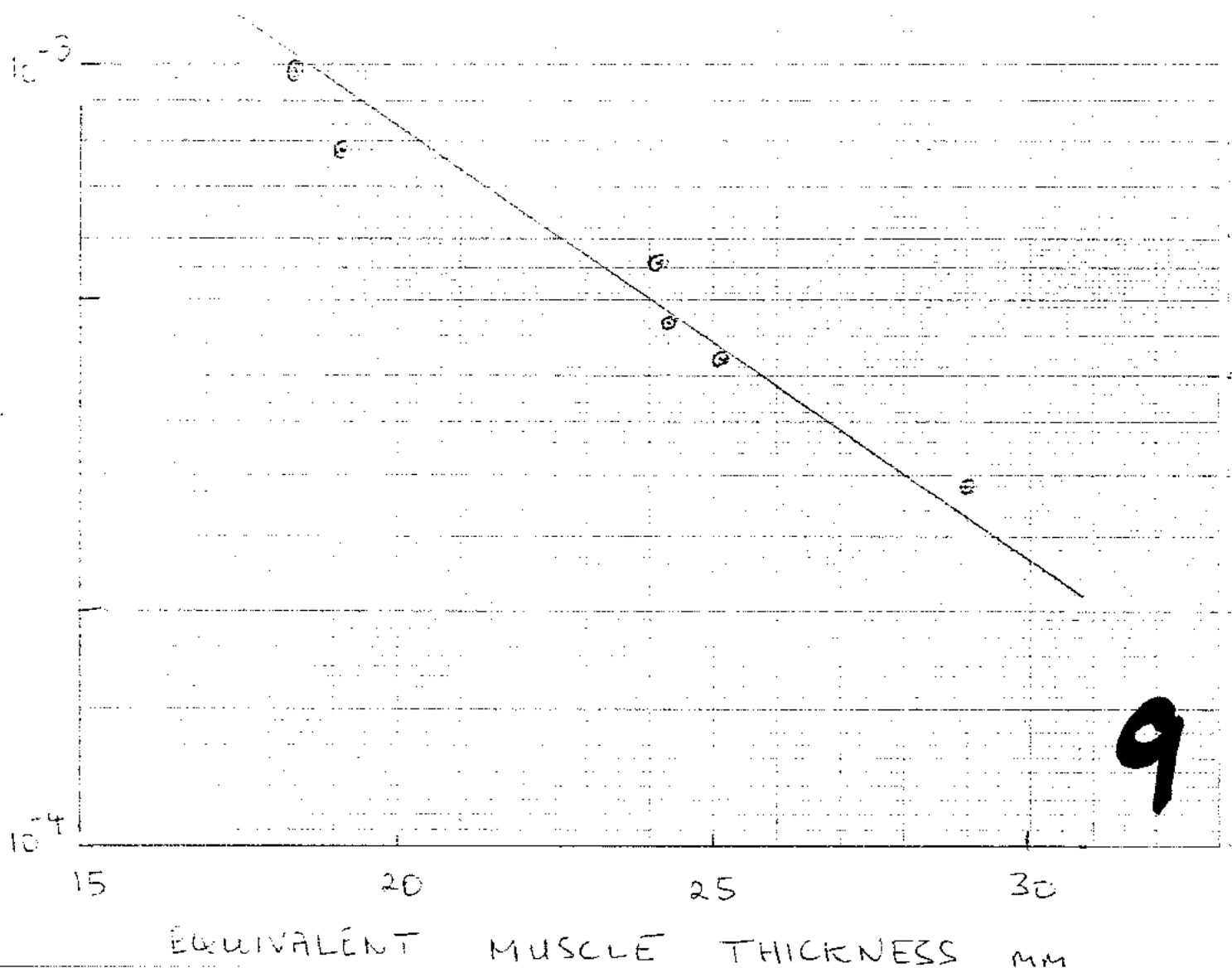
TABLE 10

PERFORMANCE OF THE PHANTOM IN PREDICTING X-RAY DETECTION
EFFICIENCIES: SUMMARY OF DATA FOR SEVEN SYSTEMS

	DETECTOR SIZE	LAB	DATA IN TABLE NO.	MEAN OBS/PRED EFFICIENCY RATIO (1)*	(2)*
PAIRED DETECTORS	114 mm dia.	LLNL	6	1.00±0.21	0.85±0.18
"	127 mm dia.	PNL	6	0.82±0.23	0.70±0.19
"	200 mm dia. (GEOMETRY 2)	HARWELL	7	1.19±0.18	1.02±0.16
"	"	ANL	7	0.92±0.20	0.79±0.19
"	150 mm x 150 mm	LLNL	6, 7	0.99±0.11	0.86±0.10
"	MEAN			0.98	0.84
SINGLE DETECTOR	200 mm dia. (GEOMETRY 1)	HARWELL	8	1.72±0.33	1.46±0.25
"	"	ANL	8	1.09±0.37	0.93±0.32

* (1): mean CWT data from three laboratories (Table 4) adopted

  (2): mean CWT data from AWRE and from PNL (Table 4) adopted

DETECTION EFFICIENCIES FOR ... IN
... 8" DIA THICKNESSES AT
HARWELL)

A. DERIVED FROM SUBJECTS WITH
¹⁰³Pd

B. DERIVED FROM SUBJECTS WITH
⁹²mNb

PHANTOM +
²³⁵Pu IN LUNGS

EQUIVALENT MUSCLE THICKNESS mm
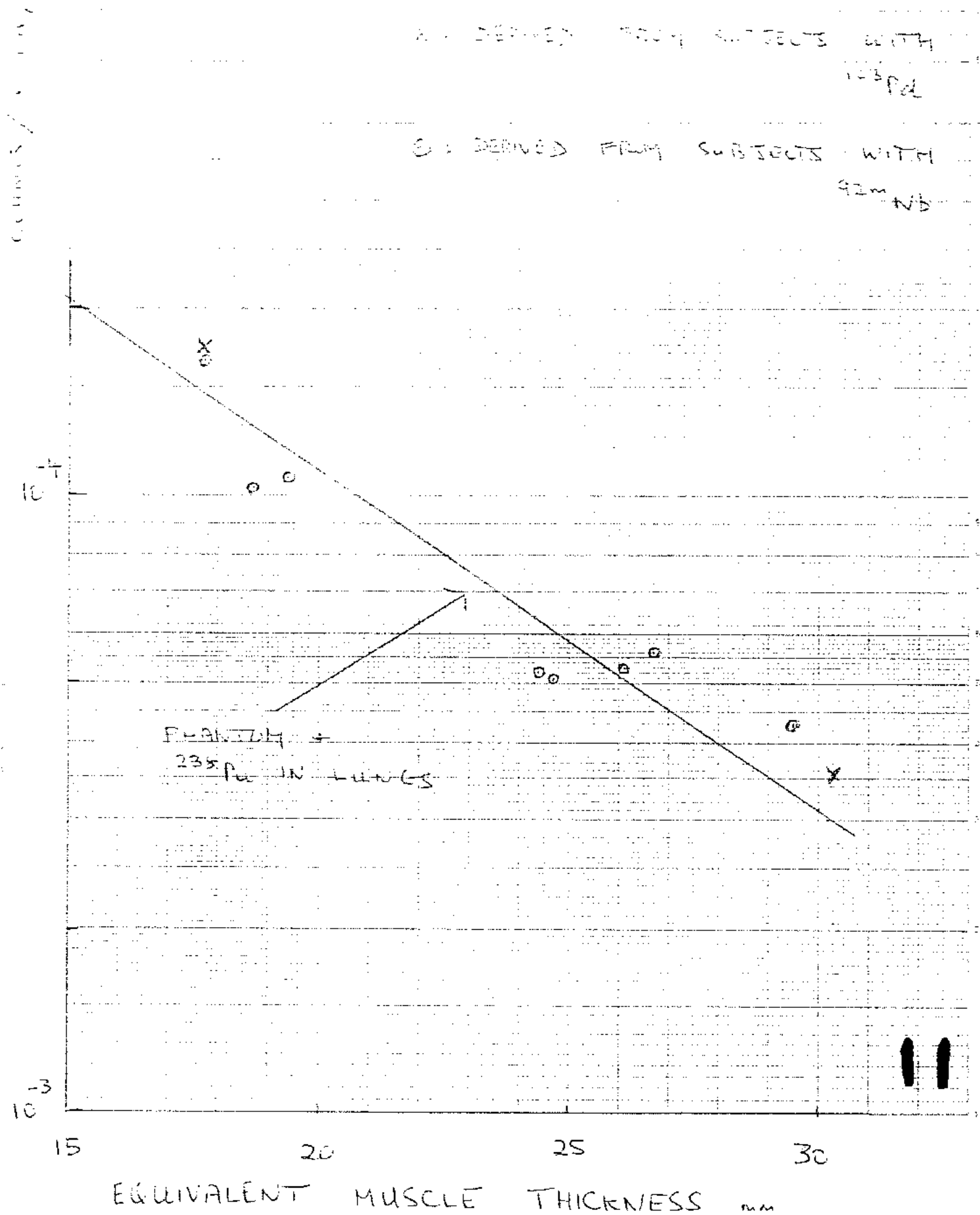
AWRE O 7/86

ATOMIC WEAPONS RESEARCH ESTABLISHMENT

AWRE REPORT No. O 7/86

Calibration of X-ray Counters for Assessment of Internal Lung
Contamination, with Low Energy X-ray Emitters, in Women
Part 1: Measurements Made at AWRE Aldermaston

AWRE,
MOD(PE),
Aldermaston, Berks.

June 1986

ATOMIC WEAPONS RESEARCH ESTABLISHMENT

AWRE REPORT NO. 07/86

Calibration of X-ray Counters for Assessment of Internal Lung
Contamination, with Low Energy X-ray Emitters, in Women
Part 1: Measurements Made at AWRE Aldermaston

███████

Final Report to IAEA on Technical Contract 3362/TC

<u>CONTENTS</u>   <u>Page</u>

2

ABBREVIATIONS

The following abbreviations have been listed in this report.

AEM	Adipose Equivalent Material
AERE	Atomic Energy Research Establishment
ANL	Argonne National Laboratory
AWRE	Atomic Weapons Research Establishment
CWT	Chest Wall Thickness
CWT_e	The Exponential CWT, calculated in 2.2.2 using equation 1
EMT	Equivalent Muscle Thickness, as defined in 2.5.3, equation 7
FIS	Female Intercalibration Study
HVT	Half-Value Thickness
IPD	Initial Pulmonary Deposit
LLNL	Lawrence Livermore National Laboratory
MEM	Muscle Equivalent Material
MIS	Male Intercalibration Study
PSD	Pulse Shape Discrimination
T_E	Effective Clearance Half-Time
87A	87% Adipose/13% Muscle Equivalent Material
50A	50% Adipose/50% Muscle Equivalent Material

The subjects are referred to as subjects A, B, C, D, E, F, G, H, I, J and K.

SUMMARY

The validity of using the Lawrence Livermore National Laboratory male phantom for calibrating detectors used in the measurement of low energy X-ray emitters in the lungs of women, has been investigated at a number of laboratories in both the United Kingdom and United States. This report outlines the results of the measurements made at AWRE only. All work was funded by the IAEA under Technical Contract number 3362/TC.

1.   INTRODUCTION

1.1   Calibration of X-ray detectors

In order to estimate the internal lung deposition of a low energy X-ray emitter, in particular plutonium, using externally placed detectors, the detector must first be calibrated. The usual procedure is to use an anthropomorphic chest phantom containing lungs uniformly loaded with a known quantity of the isotope under investigation.

It is generally accepted that the Lawrence Livermore National Laboratory (LLNL) realistic chest phantom is the best available calibration phantom for the measurement of low energy X-ray emitters in the lungs of men, for paired detectors placed over the frontal region of the chest.

1.2   The LLNL phantom

The LLNL phantom was designed to represent a male thorax between the 5th cervical and 4th lumber vertebrae (2). Its dimensions were taken from a male Caucasian cadaver, 75 kg in weight, 1.77 m tall and with a chest circumference of 1.01 m. All its relevant organs and tissues are made of polyurethane loaded with varying concentrations of $CaCo_3$ to give the correct attenuation of the Uranium L X-rays produced by plutonium.

The phantom consists of a muscle equivalent torso shell, into which can be placed moulded internal structures representing the lungs, mediastinum, liver and surrounding tissues. A synthetic ribcage is incorporated into the basic torso and chestwall.

Three sets of close fitting overlays of various thicknesses and muscle-adipose compositions are available to increase the chest wall thickness (CWT) from 16 mm (the thickness of the basic chest wall in the region commonly used for routine X-ray counting) to approximately 41 mm. The three sets of overlays are:

(a)   MEM - made of muscle equivalent material (MEM).

(b)   50A - made to give the same attenuation of U L X-rays as a 50/50 mixture, by weight, of muscle and adipose.

(c)   87A - made to give the same attenuation of U L X-rays as a 13/87 mixture, by weight of, muscle and adipose.

4

Each set of overlays can therefore be used together with the basic phantom, containing lungs loaded with a known activity of the isotope under investigation to obtain calibration equations for a number of chest wall compositions. Since these overlays cover only the frontal region of the chest calibrations equations cannnot be derived for _every_ detector geometry.

These phantoms are now available commercially and have been supplied for the calibration of lung monitors around the world.

1.3   The male intercalibration study

The International Atomic Energy Agency sponsored a study by D Newton et al. (4) to validate the use of the LLNL phantom for the calibration of measurements of low energy X-ray emitters in the lungs of Caucasian men. In this male intercalibration study (MIS), 8 volunteers of various sizes inhaled ^{92m}Nb labelled polystyrene microspheres to compare measured detection efficiencies with those predicted using the phantom.

^{92m}Nb decays by electron capture with a half-life of 10.15 days, emitting Zirconium K X-rays at similar energies to those from plutonium (table 1). A high energy gamma ray is also emitted which can be used to determine the lung content and hence the X-ray emission rate, at any given time. An initial pulmonary deposit (IPD) of 37 kBq allows 4 to 6 weeks for X-ray measurements while keeping the whole body dose equivalent to below 100 μSv.

Measurements of the MIS subjects on various detection systems showed that the best agreement, between detection efficiencies for the subject and the phantom, was obtained for paired detectors placed over the upper region of the chest, with one detector either side of the sternum. The better the coverage of the upper thorax, by the detectors, the better the agreement. However the calibration data were inconsistent for a single detector placed centrally over the chest so the results proved inconclusive for this geometry.

1.4   Calibration of X-ray detectors for female measurements

The number of female radiation workers regularly monitored for internal radioisotope contamination is currently increasing. Calibration of the detectors, however, is still generally based on measurements made with the LLNL realistic _male_ phantom, even though there are considerable differences between the shape and size of the male phantom and the average Caucasian female. For example, in ICRP 23 the reference female lung sizes and volumes are about 80% those of reference man (3).

In addition, there are significant differences in the composition and thickness of the male and female chest walls. The individuality of the size and structure of the female breast leads to considerable variability in the chest wall thickness and composition in the region viewed by the detectors. This 2 to 4 fold increase in thickness across the chest is not reproduced by the phantom overlays, whose thickness varies very little over the width or length of the chest.

The differences in both the size of the torso and its internal organs and in the overlying tissue thickness, between the phantom and the average Caucasian female could invalidate the use of the LLNL male phantom

5

for the calibration of the measurement of low energy X-ray emitters in the lungs of such women.

1.5   The female intercalibration study

The female intercalibration study (FIS) was designed with two objectives:

(a)   To investigate the validity of using the LLNL male phantom for the calibration of the detectors used in the measurement of low energy X-ray emitters in the lungs of women.

(b)   To compare the relative detection efficiencies of different detector types and geometries, by measuring the subjects on a number of detection systems. Various detector geometries were included in the comparison.

It was proposed that the methods used in the MIS would be employed, with healthy female volunteers, of known CWT and composition, inhaling an aerosol of ^{92m}Nb labelled polystyrene microspheres.

The data generated by this study could be used in the development and validation of a new "female" phantom should it show the need for one. It could also provide evidence on the use of the LLNL phantom for the calibration of measurements on non-Caucasian races, in particular male Asians, who are similar in stature to the average Caucasian female (5).

Part I of the FIS report concerns mainly these measurements made at AWRE. Part II will include the results from the other participating laboratories and their intercomparison. These were unavailable at the time of writing part I, but it is anticipated that the data collection will be complete by mid 1986 for compilation of part II.

It is envisaged that parts I and II will be amalgamated in a joint scientific paper to be published at a later date.

2.   EXPERIMENTAL METHODS AND MEASUREMENTS

2.1   Subject selection

Female Caucasian subjects were selected from healthy non-smoking volunteers, to provide a range of ages, CWTs and compositions. Preliminary inhalation studies (see 2.3) gave a final selection of 11 subjects who took part in the study. One volunteer participated twice in order that she could be measured at both the UK and the USA laboratories. Each subject gave her informed consent to take part in the study.

Measurements were made on the AWRE whole body monitor to ensure that each subject's body radiation background was normal.

2.2   Assessment of the attenuating chest wall thickness

2.2.1   Measurement of the tissue thicknesses

A Unirad, real-time, B-mode sonofluoroscope, fitted with a 5 MHz transducer, was used to measure the CWT and composition for each detector geometry and each subject. The transducer was angled to give the sharpest image - this was found to be when the transducer head was parallel to the

lung surface. The approximate points used for each detector geometry are shown in figure 1.

The measurement points were chosen at approximately midway between the ribs, where the image of the lung surface was brightest. At each point the tissue thicknesses measured were:

(a) The total chest wall thickness.

(b) The thickness of the subcutaneous adipose layer plus any additional adipose tissue observable in and between the breast and muscle tissue layers.

(c) The thickness of the total breast tissue and its glandular component.

Reference to attenuation data (9) suggested that glandular tissue is approximately muscle equivalent. Simple addition of the equivalent tissue layers therefore enabled the total CWT to be separated into total muscle equivalent tissue (muscle + glandular breast) and total adipose tissue (subcutaneous adipose + additional adipose) for each measurement point.

The percentage total adipose tissue in the CWT was estimated for each subject detector geometry.

2.2.2 Assessment of the equivalent tissue thicknesses

From the measured tissue thicknesses an exponential chest wall thickness (CWT_e), was calculated for each subject detector geometry using equation 1, as in the MIS (4). However, an adipose tissue content of 45% was taken, instead of the 30% previously used for men, due to the increased adipose equivalent tissue found in the female chest wall. The expression for CWT_e is:

$$CWT_e = \frac{-1}{\mu} \ln \left[\frac{\sum_{j=1}^{j=n} \exp(-\mu.x_j)}{n} \right] \qquad \ldots(1)$$

where n is the number of measurements of x_j, the CWT at position j and μ is the linear attenuation coefficient, calculated for a chest wall composition of 45% adipose and 55% muscle equivalent tissues, using the weighted mean linear attenuation coefficient for the two X-rays.

Since the Zr K X-rays are emitted at two different energies it is possible to calculate exponential average thicknesses of total muscle equivalent and total adipose tissues at each energy using equation 2:

7

$$T_i = \frac{-1}{\mu_i} \ln \left[\frac{\sum_{j=1}^{j=n} \exp(-\mu_i t_j)}{n} \right] \qquad \ldots (2)$$

where n is the number of measurements of t_j, the tissue (muscle or adipose) thickness at position j, μ_i is the linear attenuation coefficient of the tissue at the ith X-ray energy and T_i is the exponential tissue thickness for the energy. The linear attenuation coefficients are given in table 1 for the given tissue types and X-ray energies. The X-rays from [239]Pu, as well as [92m]Nb, are given for comparison.

The values of T_i can then be combined with the relative abundances of the X-rays to give the effective thickness of the given tissue, for both X-rays, using equation 3.

$$T_{eff} = \frac{\sum_{i=1}^{i=2} f_i \mu_i T_i}{\sum_{i=1}^{i=2} f_i \mu_i} \qquad \ldots (3)$$

where f_i is the relative abundance of the Zr K X-ray of the ith energy and T_{eff} is the effective thickness of the given tissue.

Using this method the effective tissue thicknesses for both the K_α and K_β X-rays could be calculated separately for each subject detector geometry. This is important for the germanium detection systems which readily resolve the X-ray photopeaks.

2.3 Inhalation techniques

All inhalations were administered at AERE.

2.3.1 ^{99m}Tc inhalation

In order to estimate the optimum amount of [92m]Nb activity for each inhalation, each subject first inhaled an aerosol of ^{99m}Tc labelled polystyrene microspheres. Standard inhalation techniques were used to administer the aerosol as in the MIS (4,8). The results of the ^{99m}Tc study enabled us to pair the subjects so that enough [92m]Nb activity was produced for two subject inhalations. This more economic use of the [92m]Nb saved time and costs while minimising the dose to each subject.

8

2.3.2 ^{92m}Nb production and inhalation

The ^{92m}Nb was produced by alpha particle irradiation of yttrium in the AERE variable energy cyclotron. The activity was then incorporated into a monodisperse aerosol of polystyrene microspheres using the methods previously used in the MIS (1,4).

The aerosol was administered using standard inhalation techniques as documented (4,8). After the inhalation each subject was measured at the AERE whole body monitor to ensure that the total deposition was sufficient to produce the IPD required (18 to 37 kBq depending on CWT). Seven subjects required an additional inhalation after more material was cleared than predicted.

For subject F's first inhalation, insufficient particulate activity remained to increase the IPD to the required value. It was therefore not possible to measure her at any of the US laboratories. However, a second inhalation two years later proved more successful, allowing her to participate in the complete measurement programme. This programme is summarised in table 2.

2.4 Gamma ray measurements

2.4.1 Measurement of gut clearance

The particles which are deposited in the tracheo-bronchial region are removed by ciliary clearance up the trachea and into the gut, from where they are excreted. The lung clearance is completed in approximately 24 hours in subjects with a normal lung function, whilst the gut clearance can take from 1 to 5 days to complete.

In order to monitor the progress of gut clearance a collimated NaI(Tl) detector was used to scan longitudinally over the upper part of the body to measure the distribution of the activity in the subject after the inhalation. The count-rate in the 934 keV gamma ray photopeak was recorded for 12 increments of approximately equal length. If clearance from the gut was incomplete, the scan appeared asymmetrical with increased counts towards the lower abdomen.

Low energy X-ray counting was not started until it was confirmed that activity remained only in the lungs, ie, gut clearance had been completed.

2.4.2 Assessment of clearance rate and initial pulmonary deposit

In order to calculate the X-ray emission from a subject's chest at any given time, the amount of activity present in the lungs at that time must be known. Serial measurements of the 934 keV gamma rays, over a period of up to 100 days after the inhalation, using the CsI(Tl) crystals of two phoswich detectors placed equidistant above and below the subject's chest enabled the effective clearance half-time (T_E) to be determined.

Equation 4 relates the X-ray emission at a given time post inhalation to the IPD, using the estimate of T_E from AWRE gamma ray measurements. ANL's estimates of lung content were used to estimate the IPD, due to their more accurate calibration for the gamma ray measurement (7). The lung content, $N_{(t)}$, at time t days after the inhalation is:

$$N_{(t)} = N_{(0)} \exp \left[\frac{-0.693\ t}{T_E} \right] \qquad \ldots(4)$$

where T_E is the effective clearance half-time in days and $N_{(0)}$ is the IPD.

2.5   X-ray measurements

The X-ray emissions from each subject were investigated for a number of detector geometries for both the phoswich and the germanium detection systems. In each case the detectors were positioned tangentially to a line passing across the sternal notch. For the "double" and "central" geometries each detector was orientated to secure the greatest possible area of contact with the subject's chest.

With the phoswich detection system, measurements of the X-ray emissions were also assessed using one detector positioned over the left or right lung. The detector was oriented at the angle used for the "central" geometry, with the detector displaced one detector half-width to the side of measurement. The responses for the two measurements (left + right) were then summed to compare the detection efficiencies for this geometry and the more angled "double" geometry. Figure 2 shows the differences in detector positioning for these two double detector counting geometries.

A number of geometries were investigated to detect the X-ray emissions from the side of the thorax (under the armpit). Ultrasonics data suggested that greater X-ray detection efficiencies would be obtained due to the thinner CWT in this region. Two different detector geometries were used, one with the subject lying with the side of measurement uppermost and the other with the subject seated and the arms raised to shoulder level.

Count-rates from the back, using single or paired detectors, with the subjects' arms up or down, were also measured in some cases.

Figure 1 summarises the geometries investigated. Where possible several measurements of the X-ray emissions were made for each geometry in an attempt to minimise any errors due to reproducibility of detector positioning. Count times were selected to try to give less than 1% error due to counting statistics without causing discomfort to the subjects.

2.5.1.   Phoswich measurements

The detectors used at AWRE were 200 mm in diameter and comprised a 1.5 mm thick NaI(Tl) crystal backed by a 50 mm thick CsI(Tl) crystal. The beryllium entrance window was 0.25 mm thick.

The phoswich spectrum acquired from a subject with ^{92m}Nb in the lungs showed the counts from X-ray emissions superimposed upon the scattered quanta from the 934 keV gamma ray. In order to estimate the X-ray detection efficiency in the energy region of interest (11 to 23 keV), it was necessary to distinguish the X-ray counts from the scattered counts.

A method using a repeat measurement with copper sheets, interposed between the detector and the subject, to remove the majority of the X-ray counts and thus provide an estimate of the scattered counts was

described by Newton et al. (4). Because the copper sheet also attenuates this scattered quanta in the energy region of interest, it was then necessary to perform an extrapolation upon the residual spectrum produced by subtracting the results of a repeat X-ray measurement.

An alternative method was employed by AWRE. This involved interpolation, using the spectral data from higher and lower energy regions about the X-ray peak to estimate the baseline. This had the advantage of only requiring a single measurement and therefore eliminated any problems of reproducibility that could have occurred with a repeat measurement.

Due to the anti-coincidence feature of the phoswich and the pulse shape discrimination (PSD) circuits which this entails, losses in X-ray counting efficiency occurred. These could be estimated by observing the response to a ^{92m}Nb point source, with and without PSD. In order to make comparisons between measurements made over a period of time and at different laboratories all the X-ray count data were adjusted to values assuming 100% efficiency.

An additional complication, which was caused by the relatively high gamma ray flux, was the loss of low energy pulses due to dead-time effects, ie, X-ray pulses were not detected if they reached the PSD circuits too close in time to the pulses from the 934 keV gamma rays. This was investigated using a similar technique to that described by Newton et al.(4), who also observed this effect. The X-ray count data were therefore further adjusted to allow for the losses due to dead time.

2.5.2 Germanium measurements

Each germanium array comprised six hyperpure germanium planar detectors arranged in a 3 by 2 matrix. Each detector had a sensitive thickness of 8 mm, a sensitive area of 1500 mm and was recessed in the housing approximately 20 mm behind a Mylar window. Their separation (centre to centre) was 65 mm.

Interpretation of the X-ray count data obtained using the germanium detection system was made much simpler by the improved resolution, with the two X-ray photopeaks clearly distinguishable. A choice of well established and generally simpler techniques are available to calculate the baseline beneath the X-ray photopeaks. At AWRE, a method based upon a 5 point smooth was used to analyse the summed spectrum from the 6 elements of the germanium array. Count data for the K_α, K_β and $K_{\alpha+\beta}$ photopeaks were all obtained. However, only the $K_{\alpha+\beta}$ data are presented here. Further analysis is required to provide more conclusive data on the separate K_α and K_β emissions.

2.5.3. Calibration with the LLNL phantom

In the manufacture of the niobium labelled particles, excess ^{92m}Nb activity was produced. This was used to manufacture several sets of labelled polyurethane lungs using techniques developed at AWRE. The concentration of ^{92m}Nb in the right and left lungs was based on the mass ratio of the lungs and was 1.0:0.8 (R:L).

The ^{92m}Nb labelled lungs were used in the LLNL phantom to derive calibration equations for a number of detector geometries. Equation 5 gives the typical format of a calibration equation:

11

$$E_{Nb} = Y.exp \left[\frac{-Z}{HVT} \right] \qquad \qquad ...(5)$$

where HVT is the half-value thickness and Y and Z are constants, for the given geometry and CWT composition. E_{Nb} is the detection efficiency in counts detected per Zr K X-ray emitted in the lungs. Equations were derived for both the MEM overlays and the 87A overlays, for each geometry. As far as possible an effort was made to reproduce the same detector/thorax configurations as had been used for the subject measurements. Several measurements were made for each overlay, in each geometry, to minimise errors due to repositioning of the detectors.

In order to predict the detection efficiencies for each detector geometry, using the relevant calibration equations, it was necessary to relate the muscle equivalent chest wall thickness of the phantom to the ultrasonic measurements made on each subject. This could be achieved by first calculating the half-value thickness for a material which was equivalent to wholly adipose tissue (adipose equivalent material or AEM). This value could then be related to the half-value thicknesses measured for the MEM and 87A overlays using equation 6:

$$HVT_{(AEM)} = \frac{HVT_{(87A)} \cdot HVT_{(MEM)}}{1.15 \ HVT_{(MEM)} - 0.15 \ HVT_{(87A)}} \qquad ...(6)$$

Using the half-value thicknesses for AEM and MEM the equivalent muscle thickness (EMT) could be calculated for each subject in each detector geometry. This is defined to be the chest tissue thickness equal to the phantom muscle equivalent CWT which would produce the same detection efficiency as the appropriate combined thicknesses of MEM and AEM, as given by equation 7:

$$EMT = \frac{HVT_{(MEM)} \cdot T_A}{HVT_{(AEM)}} + T_M \qquad ...(7)$$

where T_A and T_M are the subject's effective tissue thicknesses (T_{eff}) of adipose and muscle respectively, derived from the ultrasonic measurements using equations 2 and 3.

2.6   Inhalation dose assessment

The total radiation doses received by the whole body and individual identified organs were calculated for each volunteer. The dose estimates were based upon the total activity inhaled, the IPD and the clearance half-times.

3.   RESULTS

3.1   Subject variation

Eleven female subjects were selected from over 20 volunteers. The selection was made to give a wide range of ages, subject sizes, and chest wall parameters as shown in table 3. It was noted that the percentage adipose tissue varied very little between the subjects, the mean being

12

43%, with a standard deviation of 3%. The chest wall values listed are for the 200 mm diameter double geometry.

3.2   The inhalations

The percentage deposition in the alveolar region was found to be lower for females than for males. Preliminary studies indicated a 25% smaller deposition of the 5 μm microspheres in women compared to men (approximately the same as the difference in airway diameter between the sexes).

As the detection of the low energy X-rays from the lungs is dependent upon the distribution within the lung any variation in the deposition pattern may affect the observed detection efficiencies. The FIS was therefore suspended after the first year while we used ^{99m}Tc to study the effect of particle size on alveolar deposition in females. By this time six subjects (A, B, C, D, E and F) had participated in the FIS.

This study financed by AWRE and carried out at AERE, took a year to complete. The results were presented at the second International Workshop on Lung Dosimetry in September 1985 (5).

From the results of this technetium study it was decided to decrease the particle size for the final 6 subjects (F, G, H, I, J and K), to 3.5 μm - the particle size which gives the same deposition in women as the 5 μm aerosol does in men. Some of the final 6 subjects were matched to be of similar CWT to the first 6 subjects in order to compare the counting efficiencies for the different particle sizes. One subject, F, was in each group and therefore inhaled both aerosol sizes.

3.3   Clearance half-times and initial pulmonary deposits

After inhalation of the ^{92m}Nb each subject was scanned with a collimated NaI(Tl) detector to determine whether gut clearance was complete. Figure 3 shows the results of two scans made on subject A. The first scan, made on day 1 showed an increase in the count-rate towards the lower abdomen, confirming that gut clearance was incomplete. The second scan, taken on day 5, had a symmetrical countrate distribution suggesting that the majority of the remaining activity was present in the region of the lungs. It was then appropriate to commence low energy X-ray counting. This pattern was observed with each subject, early gut clearance taking on average 4 to 5 days.

The effective and biological clearance half-times were calculated for each subject based on serial measurements of the 934 keV gamma ray emissions. These values, together with the estimates of IPD obtained from ANL measurements, are summarised in table 4. Figure 4 shows the clearance half-time plot for subject D.

3.4   X-ray measurements

Calibration equations were derived for a number of detector geometries on both the phoswich and germanium detection systems, using the LLNL phantom with the MEM and 87A overlays. A complete list of the HVTs, used to calculate each subject's EMT, can be found in table 5. All the calibration equations, based on measurements made with the MEM overlays, are listed in table 6. Figure 5 shows the calibration curves, for a 200 mm

13

diameter phoswich detector, positioned over the right chest of the LLNL phantom.

Phoswich spectra of the type shown in figure 6 were obtained for each subject, for as many detector geometries as possible. The example shown is from a 10 minute count made on subject D, with a 200 mm diameter phoswich in the central geometry. Similarily, germanium spectra of the type shown in figure 7 were also obtained. This spectrum, from a 30 minute count on subject D, shows the summed response from the 12 elements of the two germanium arrays, positioned in a double geometry.

The calibration equations from table 6 were used to calculate the predicted detection efficiencies for each subject. These values could then be compared with the subject measurements to evaluate the validity of the phantom for each detector geometry. Figures 8 and 9 show graphically this comparison for the central germanium and double phoswich geometries. From the scatter of the points about the calibration line it can be deduced that there is a good agreement between the observed and predicted detection efficiencies for the central germanium geometry. However, this does not appear to be the case for the double phoswich geometry, where most of the results were less than those predicted with the calibration equations.

Tables 7 to 11 give a complete summary of all the results for both the phoswich and germanium detection systems. Each subject's observed and predicted detection efficiencies are listed together with the ratio (observed:predicted).

A number of detector geometries were investigated for measurements at the sides of the thorax, below the armpit. Since the phantom overlays do not extend to these regions it was not possible to obtain any calibration equations. No predicted detection efficiencies could therefore be calculated for the subjects. However, a comparison could be made with the detection efficiencies for other geometries. Tables 12 to 14 list the observed detection efficiencies for the side and central geometries.

A small number of measurements were also made at the back of some subjects. These observed detection efficiencies have also been compared with those from the central geometry and are listed in table 15.

3.5   Inhalation dose estimates

The total organ and whole body dose equivalent estimates are given in table 16.

4.   CONCLUSIONS

A summary of the results for both the phoswich and germanium detection systems can be found in table 17. It would appear that the best agreement between the observed and predicted detection efficiencies is obtained for the central geometries.

Despite this good agreement there were occasionally large differences between the observed and predicted detection efficiencies. This was particularly the case for subject B on the germanium system, with the ratio (observed:predicted) as large as 2.4. This is reflected by standard deviations of 40% about the mean ratio for the phoswich system and 60% for the germanium system.

14

Large discrepancies were observed for the double geometries which are commonly used to assess the plutonium lung content in both men and women. This may be due, in part, to the variation in the CWT across the female chest which is not reproduced by the phantom.

A considerable difference was observed between the mean ratio obtained for the standard (angled) double phoswich geometry and the summed response for the left and right geometries. On average detection efficiencies were 40% greater for the latter, L + R, geometry. This is most probably due to the detectors being closer to the thinnest regions of the chest wall in this geometry (figure 2).

The improvement in the detection efficiency obtained from monitoring the sides of the thorax, under the armpit, was dependant upon the specific detector type and geometry used. When the subjects were lying on one side, with the side of measurement uppermost, the improvement in detection efficiency, compared to that obtained for the central geometry, was on average 40% for the germanium system and 100% for the phoswich system. However, for the small number of subjects monitored sitting up, with the phoswich system, no improvement over the central detector geometry was observed.

The few measurements made from the back showed that there was no advantage to be gained from this geometry.

Since, at the present time, only the measurements made at AWRE have been analysed, it would be unfair to draw too many conclusions. A more complete evaluation of the use of the LLNL phantom will be given when the data from the other laboratories participating in the FIS have been analysed.

REFERENCES

1.   R C Fleming: "The Production of Niobium-92m Labelled 5 μm Diameter Polystyrene Microspheres". AERE R-9670 HMSO (1980)

2.   R V Griffith, P N Dean, A L Anderson and J C Fisher: "A Tissue Equivalent Torso Phantom". In: Advances in Radiation Protection Monitoring, 493-504, IAEA, Vienna (1979)

3.   International Commission of Radiological Protection, Publication 23: Report of the Task Group on Reference Man. Pergamon Press, Oxford (1975)

4.   D Newton et al.: "The Livermore Phantom as a Calibration Standard in the Assessment of Plutonium in Lungs". AERE R-11201, HMSO (1983)

5.   J N Pritchard, S J Jefferies and A Black: "Regional Deposition of 2.5 to 5.0 μm Polystyrene Microspheres Inhaled by Women". Presented at the 2nd International Workshop on Lung Dosimetry, 6th International Symposium on Inhaled Particles, Cambridge, UK. September 1985.

6.   G I Tanaka, H Kawamura and T Nomura: "Physical Characteristics of the Japanese in Relation to Reference Man". In: Radiation Protection. A systematic approach to safety. 288-291. IRPA, Washington DC, USA (1980)

7.   R E Toohey, A L Keane and J Rundo: "Measurement Techniques for Radium and the Actinides in Man at the Center for Human Radiobiology". Health Physics 44, Supplement 1, 323-341 (1983)

8.   M Walsh, A Black and N Foord: "Apparatus For The Administration by Inhalation of Radioactive Particles to Human Subjects for Studies of Deposition and Clearance". J Aerosol Science 8 83-90 (1977)

9.   D R White and C Constantinou: "Anthropomorphic phantom materials". In: Progress in Medical Radiation Physics, Chapter 3. Plenum (1982)

TABLE 1

X-Ray Emissions From 92m-Niobium and 239-Plutonium and Their Linear Attenuation Coefficients for Muscle and Adipose Tissues

Nuclide	X-Ray Series	Energy (keV)	Abundance (%)	Linear Attenuation Coefficients* Muscle (cm⁻¹)	Adipose (cm⁻¹)
239 Plutonium	U L_α	13.6	1.67	1.98	1.07
	U L_β	17.2	2.38	1.02	0.60
	U L_γ	20.2	0.55	0.69	0.43
92m Niobium**	Zr K_α	15.8	53.6	1.29	0.73
	Zr K_β	17.7	9.9	0.95	0.56

**92m Nb also emits a gamma ray at 934 keV (99.15% abundance)

*Sum of coefficients for the photoelectric absorption and Compton scattering based on calculations by ███████ cf D Newton report (4)

TABLE 2

Timetable of Measurements Following Each Inhalation

Day 1	Inhalation at AERE, followed by measurements on the Whole Body Monitor to ensure adequate lung content
Day 2 - 5	Completion of early lung and gut clearance checked by gamma scans
Day 5 - 15	Daily gamma counting at AWRE to determine lung clearance rate. X-ray counting at UK laboratories to determine detection efficiencies with different detection systems
Day 17 - 30	X-ray counting at US laboratories, with 2 to 3 days at each laboratory
Day 34 onwards	Further gamma measurements at weekly to monthly intervals

TABLE 3

Details of the Subjects
(200 mm Phoswich Double Geometry)

Subject	Age	Height, m	Weight, kg	CWT, mm	PAT, %	EMT, mm	CC, mm
A					38	31	890
B					45	25	1002
C					41	27	964
D					41	19	775
E					41	22	876
F 1					45	36	1011
F 2					50	39	1074
G					43	17	835
H					38	33	952
I					42	25	839
J					46	30	926
K					43	17	865
Mean	37 ± 12	1.63 ± 0.05	67 ± 12	33 ± 9	43 ± 3	27 ± 7	917 ± 87

CWT - Chest Wall Thickness, exponential average assuming 45% adipose

PAT - Percentage Adipose Tissue in the chest wall

EMT - Phantom Equivalent Muscle Thickness of the chest wall

CC - Chest Circumference

Age range	23 - 51 years
Weight range	53 - 90 kg
CWT range	21 - 50 mm
EMT range	17 - 39 mm

TABLE 4

Initial Pulmonary Deposition and Clearance Half-Time Estimates

Subject	IPD$^\oplus$, kBq	IPD$^\ominus$, kBq	Effective Half-life, T_E, days$^\boxtimes$	Biological Half-life, days$^\boxtimes$
*A	23	27	8.89 ± 0.09	71 ± 6
*B	4	17	9.15 ± 0.09	93 ± 8
*C	16	21	8.65 ± 0.08	58 ± 4
*D	36	-	9.10 ± 0.10	88 ± 10
*E	< 4	9	9.84 ± 0.03	324 ± 35
*F 1	14	-	9.34 ± 0.05	118 ± 8
+F 2	33	39	9.53 ± 0.03	155 ± 8
+G	17	-	9.59 ± 0.04	174 ± 12
+H	19	61	9.77 ± 0.04	263 ± 30
+I	33	-	9.28 ± 0.11	108 ± 15
+J	30	43	9.49 ± 0.03	145 ± 8
+K	26	-	9.90 ± 0.12	402 ± 16

Average effective clearance half-times:

Female
5 μm (*)   9.16 ± 0.41
3.5 μm (+)   9.59 ± 0.22

Male
5 μm (8 subjects)   9.65 ± 0.26

$^\oplus$Initial Inhalation

$^\ominus$Total IPD after inhalation

$^\boxtimes$1 SD errors from weighted least squares fit

Clearance half-time based on measurements made at AWRE (NRPB for FAF). IPD based on measurements made at ANL with AWRE clearance half-time.

TABLE 5

Half-Value Thicknesses From The
LLNL Phantom Calibration

Detector Geometry	HVT (MEM), mm	HVT (87A), mm	HVT (AEM), mm
1. The Phoswich System			
(a) Central	4.5	6.9	(7.5)
(b) L + R	4.4	7.3	(8.1)
(c) Double	4.5	7.1	(7.8)
2. The Germanium System			
(a) Central	4.6	7.0	(7.6)
(b) Double (12 elements)	4.3	6.9	(7.6)
(c) Double (10 elements)	4.5	7.2	(7.9)

Figures in parentheses are interpolated estimates using equation 6

TABLE 6

LLNL Phantom Calibration Equations For The
AWRE Detection Systems

Detector Geometry	Calibration Equation
1. The Phoswich System (a) Central	$E_{Nb} = 8.30 \exp\left[\dfrac{-0.693\ EMT}{4.5}\right]$
(b) L + R	$E_{Nb} = 13.28 \exp\left[\dfrac{-0.693\ EMT}{4.4}\right]$
(c) Double	$E_{Nb} = 17.94 \exp\left[\dfrac{-0.693\ EMT}{4.5}\right]$
2. The Germanium System (a) Central	$E_{Nb} = 1.72 \exp\left[\dfrac{-0.693\ EMT}{5.2}\right]$
(b) Double (12 elements)	$E_{Nb} = 2.05 \exp\left[\dfrac{-0.693\ EMT}{4.3}\right]$
(c) Double (10 elements)	$E_{Nb} = 1.52 \exp\left[\dfrac{-0.693\ EMT}{4.5}\right]$

E_{Nb} = Counting efficiency, counts per 1000 K X-rays emitted in the lungs

TABLE 7

Predicted And Observed Detection Efficiencies-
200 mm Phoswich Central Geometry

Subject	EMT	Observed E_{Nb} ⊗	Predicted E_{Nb} ⊗	Ratio Obs/Pred
A	26	2.0 ± 0.2 (8)*	1.5	1.33
B	22	1.6 ± 0.1 (4)	2.8	0.57
C	24	1.8 ± 0.2 (6)	2.1	0.86
D	15	3.7 ± 0.4 (6)	8.2	0.45
E	18	3.7 ± 0.4 (4)	5.2	0.71
F 1	31	0.9 ± 0.1 (5)	0.7	1.29
F 2	39	0.3 ± 0.1 (3)	0.2	1.50
G	15	5.2 ± 0.7 (4)	8.2	0.63
H	31	1.0 ± 0.2 (9)	0.7	1.43
I	20	1.7 ± 0.2 (6)	3.8	0.45
J	24	2.3 ± 0.1 (3)	2.1	1.10

5 μm subjects mean: 0.87 ± 0.37

3.5 μm subjects mean: 1.02 ± 0.47

all subjects mean: 0.94 ± 0.40

⊗Counts per 10^{-4} Zr K X-rays

*Number of measurements made

TABLE 8

Predicted And Observed Detection Efficiencies-
200 mm Phoswich Left + Right Geometry

Subject	EMT	Observed E_{Nb} ⊗	Predicted E_{Nb} ⊗	Ratio Obs/Pred
A	30	2.4 (2)*	1.2	2.00
B	25	1.9 (1)	2.6	0.73
C	26	2.4 ± 0.4 (4)	2.2	1.09
D	18	4.5 ± 0.7 (3)	7.8	0.58
E	22	4.9 ± 0.4 (3)	4.2	1.17
F 1	35	1.2 ± 0.1 (4)	0.5	2.40
F 2	39	0.5 ± 0.1 (4)	0.3	1.67
G	17	6.0 ± 0.4 (3)	9.1	0.66
H	33	1.1 ± 0.2 (7)	0.9	1.22
I	25	1.6 ± 0.5 (5)	2.6	0.62
J	29	3.1 (2)	1.4	2.21

5 μm subjects mean: 1.33 ± 0.72

3.5 μm subjects mean: 1.28 ± 0.68

all subjects mean: 1.30 ± 0.67

⊗Counts per 10^{-4} Zr K X-rays

*Number of measurements made

TABLE 9

Predicted And Observed Detection Efficiencies- 200 mm Phoswich Double Geometry

Subject	EMT	Observed E_{Nb} ⊗	Predicted E_{Nb} ⊗	Ratio Obs/Pred
A	31	1.4 ± 0.3 (8)*	1.5	0.93
B	25	1.1 ± 0.1 (4)	3.8	0.29
C	27	1.6 ± 0.2 (4)	2.8	0.57
D	19	4.5 ± 0.5 (3)	9.6	0.47
E	22	3.9 ± 0.1 (3)	6.1	0.64
F 1	36	1.0 ± 0.2 (4)	0.7	1.43
F 2	39	0.1 (2)	0.4	0.25
G	17	4.4 ± 0.1 (3)	13.1	0.34
H	33	0.7 ± 0.2 (7)	1.1	0.64
I	25	1.4 ± 0.3 (5)	3.8	0.37

5 μm subjects mean: 0.72 ± 0.41

3.5 μm subjects mean: 0.40 ± 0.17

all subjects mean: 0.59 ± 0.36

⊗Counts per 10^{-4} Zr K X-rays

*Number of measurements made

24

TABLE 10

Predicted And Observed Detection Efficiencies-
Germanium Array Central Geometry

Subject	EMT	Observed E_{Nb} ⊗	Predicted E_{Nb} ⊗	Ratio Obs/Pred
A	26	5.0 ± 0.5 (5)*	3.4	1.47
B	30	4.6 (2)	1.9	2.42
C	23	5.7 ± 0.7 (5)	5.4	1.06
D	15	10.9 ± 1.6 (6)	18.0	0.61
E	18	13.5 ± 4.0 (3)	11.4	1.18
F 2	35	0.9 (1)	0.9	1.00
G	14	9.1 ± 3.6 (3)	20.9	0.44
H	29	2.7 (2)	2.2	1.23
I	19	3.7 ± 1.5 (7)	9.8	0.38
J	24	2.9 (2)	4.6	0.63
K	13	12.5 (2)	24.3	0.51

5 μm subjects mean: 1.35 ± 0.67

3.5 μm subjects mean: 0.70 ± 0.34

all subjects mean: 0.99 ± 0.60

⊗Counts per 10^{-6} Zr K X-rays

*Number of measurements made

25

TABLE 11

Predicted And Observed Detection Efficiencies-
Germanium Array Double Geometry

Subject	EMT	Observed E_{Nb} ⊗	Predicted E_{Nb} ⊗	Ratio Obs/Pred	
A	30	5.2 ± 1.2 (6)*	1.6	3.25	
C	28	7.9 ± 1.1 (3)	2.3	3.43	12 Ge elements
D	18	17.6 ± 1.1 (4)	11.3	1.56	
E	21	18.4 ± 5.4 (3)	6.9	2.67	
F 2	39	1.3 (2)	0.4	3.25	
G	17	12.3 ± 3.3 (4)	11.1	1.11	10 Ge elements
H	31	3.2 ± 0.4 (3)	1.3	2.46	
I	21	7.2 ± 4.4 (7)	6.0	1.20	

5 μm subjects mean: 2.73 ± 0.84 - 12 elements

3.5 μm subjects mean: 2.01 ± 1.03 - 10 elements

all subjects mean: 2.37 ± 0.95

⊗Counts per 10^{-5} Zr K X-rays

*Number of measurements made

TABLE 12

Observed Detection Efficiencies
200 mm Phoswich Thoracic Sides, Lying Geometry

Subject	Observed E_{Nb}		Central Phos. E_{Nb}
	Left	Right[⊗]	
C	2.8 ± 0.2 (3)*	2.7 ± 0.7 (3)	1.8 ± 0.2
D	6.1 ± 0.2 (2)	3.2 ± 0.9 (2)	3.7 ± 0.4
E	7.6 ± 0.8 (3)	10.5 ± 1.9 (3)	3.7 ± 0.4
F 1	0.9 ± 0.3 (4)	2.3 ± 0.5 (4)	0.9 ± 0.1
F 2	0.9 ± 0.2 (3)	1.0 ± 0.1 (3)	0.3 ± 0.1
G	5.7 ± 0.6 (3)	5.0 ± 0.2 (3)	5.2 ± 0.7
H	1.5 ± 1.0 (5)	2.4 ± 0.6 (5)	1.0 ± 0.2
I	4.7 ± 1.0 (4)	3.4 ± 0.3 (4)	1.7 ± 0.2
J	5.2 ± 0.4 (2)	7.5 ± 0.8 (2)	2.3 ± 0.1

[⊗]Counts per 10^{-4} Zr K X-rays

*Number of measurements made

TABLE 13

Observed Detection Efficiencies
200 mm Phoswich Thoracic Sides, Sitting Geometry

Subject	Observed E_{Nb}		Central Phos. E_{Nb}
	Left	Right[⊗]	
F 2	0.5 ± 0.1 (3)*	0.3 ± 0.1 (3)	0.3 ± 0.1
G	4.4 ± 0.7 (3)	3.5 ± 0.2 (3)	5.2 ± 0.7
H	0.8 ± 0.1 (6)	0.5 ± 0.1 (6)	1.0 ± 0.2
I	3.6 ± 0.6 (4)	2.8 ± 0.5 (3)	1.7 ± 0.2
J	2.4 ± 1.0 (2)	2.8 ± 0.3 (2)	2.3 ± 0.1

[⊗]Counts per 10^{-4} Zr K X-rays

*Number of measurements made

TABLE 14

Observed Detection Efficiencies
Germanium Array Thoracic Sides, Lying Geometry

Subject	Observed E_{Nb}		Central Ge E_{Nb}
	Left	Right[⊗]	
C	0.9 ± 0.3 (3)*	0.5 ± 0.2 (3)	0.6 ± 0.1
D	1.2 ± 0.3 (3)	1.5 ± 0.4 (3)	1.1 ± 0.2
E	2.4 ± 0.1 (2)	2.7 ± 0.2 (2)	1.4 ± 0.4
G	0.9 ± 0.2 (3)	1.3 ± 0.6 (3)	0.9 ± 0.4
H	0.36 (1)	0.3 (1)	0.3 ± 0.1
I	0.8 ± 0.2 (3)	0.7 ± 0.2 (3)	0.4 ± 0.2
K	1.59 (1)	1.46 (1)	1.3 ± 0.1

[⊗]Counts per 10^{-5} Zr K X-rays

*Number of measurements made

TABLE 15

Observed Detection Efficiencies
200 mm Phoswich Central Back Geometry

Subject	Observed E_{Nb}[⊗]	Central E_{Nb}
A	1.6 (2)*	2.0 ± 0.2
C	1.1 (2)	1.8 ± 0.2
D	3.5 ± 1.2 (4)	3.7 ± 0.4
I	3.4 (2)	2.0 ± 0.2

[⊗]Counts per 10^{-4} Zr K X-rays

*Number of measurements made

TABLE 16

Total Dose Estimates

Subject	92mNb Dose to Lung, μSv	92mNb Dose to Breast, μSv	92mNb Dose to Gut, μSv	92mNb Dose to Ovaries, μSv	92mNb Whole Body Equivalent Dose, μSv
A	235	46	512	94	94
B	156	31	595	111	92
C	182	36	670	125	103
D	325	62	147	20	66
E	94	19	667	126	89
F 1	124	25	422	79	67
F 2	364	70	273	48	93
G	164	31	55	8	35
H	586⊗	112⊗	417⊗	72⊗	149⊗
I	296⊗	57⊗	137⊗	23⊗	69⊗
J	418	80	367	65	118
K	255	49	78	12	58

⊗The presence of 1.5% 91mNb resulted in an additional dose of approximately 20% of that shown above

TABLE 17

Summary of the Results

Detector Geometry	Mean Ratio, Obs/Pred
Phoswich	
Central	0.94 ± 0.40
Left + Right	1.30 ± 0.67
Double	0.59 ± 0.36
Germanium	
Central	0.99 ± 0.60
Double	2.37 ± 0.95
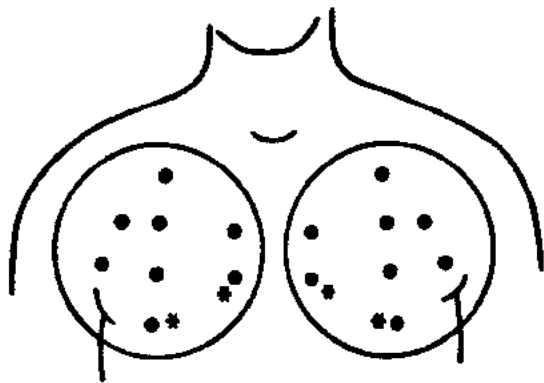
1. 200 mm Phoswich Standard
   Double Geometry
   (125 mm Standard Double Exclude * Points)
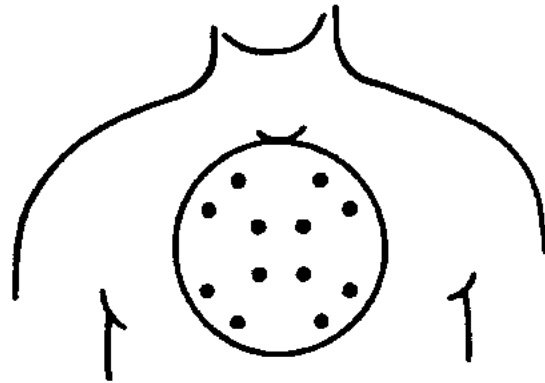
2. 200 mm Phoswich Standard
   Central Geometry
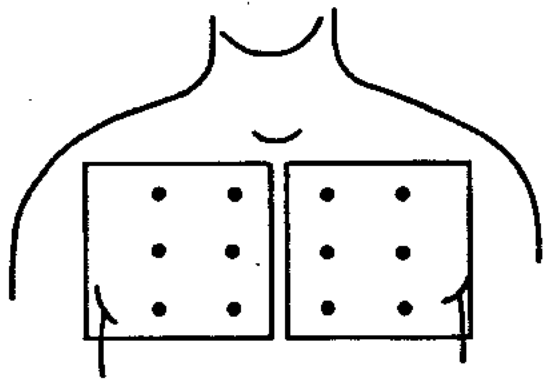
3. Germanium Array Geometries
   Standard Double - all Points
   Standard Central - Central 6 Points
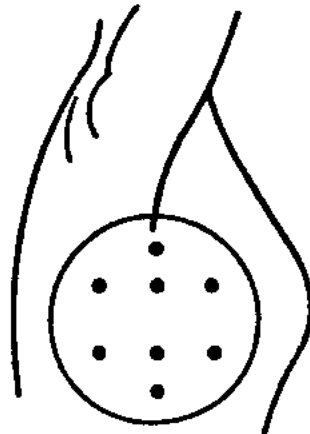
4. 200 mm Phoswich Thoracic
   Sides Geometries
   (Measured Sitting or Lying)
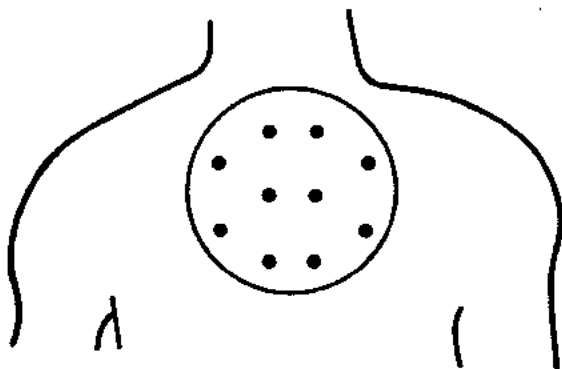
5. 200 mm Phoswich Central
   Back Geometry
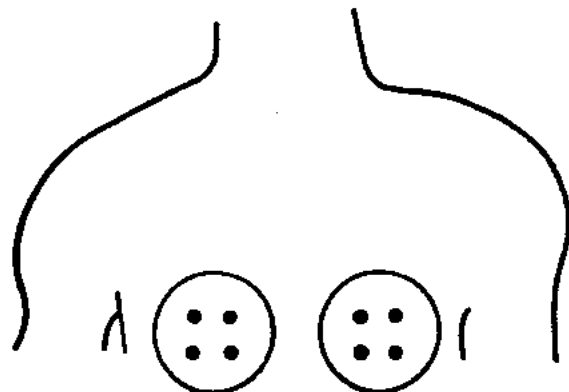
6. 125 mm Phoswich Double
   Back Geometry

FIGURE 1. ULTRASONIC POINTS OF MEASUREMENT FOR THE ASSESSMENT OF THE ATTENUATING
TISSUE THICKNESS FOR EACH COUNTING GEOMETRY
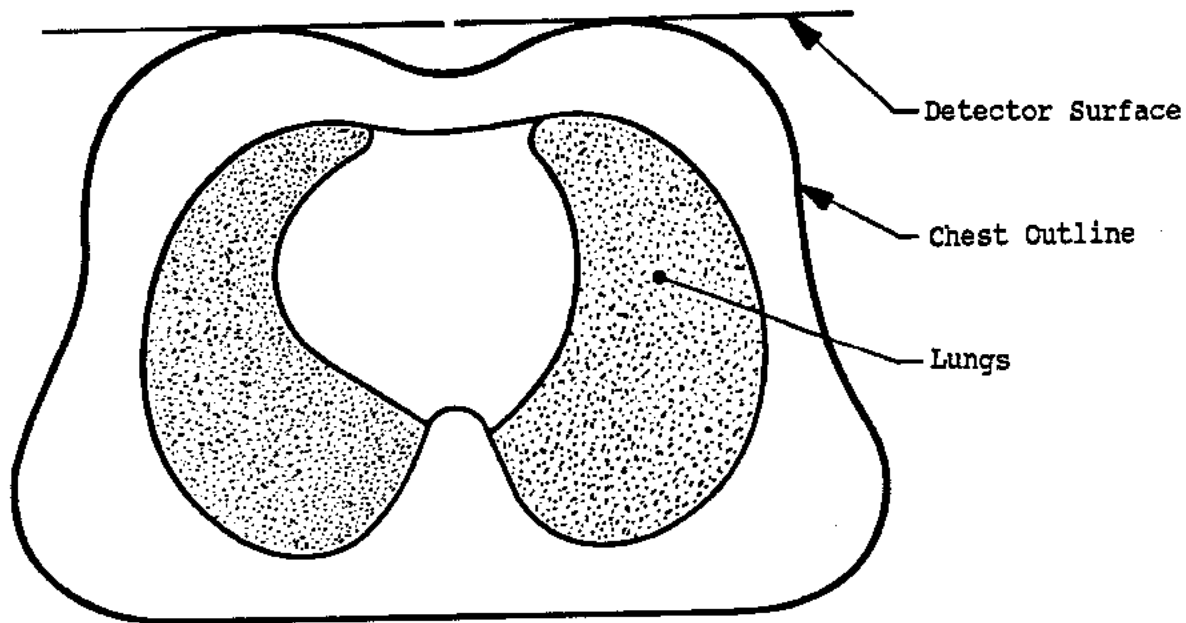
(a) Horizontal Across the Chest - L + R Detector Geometries
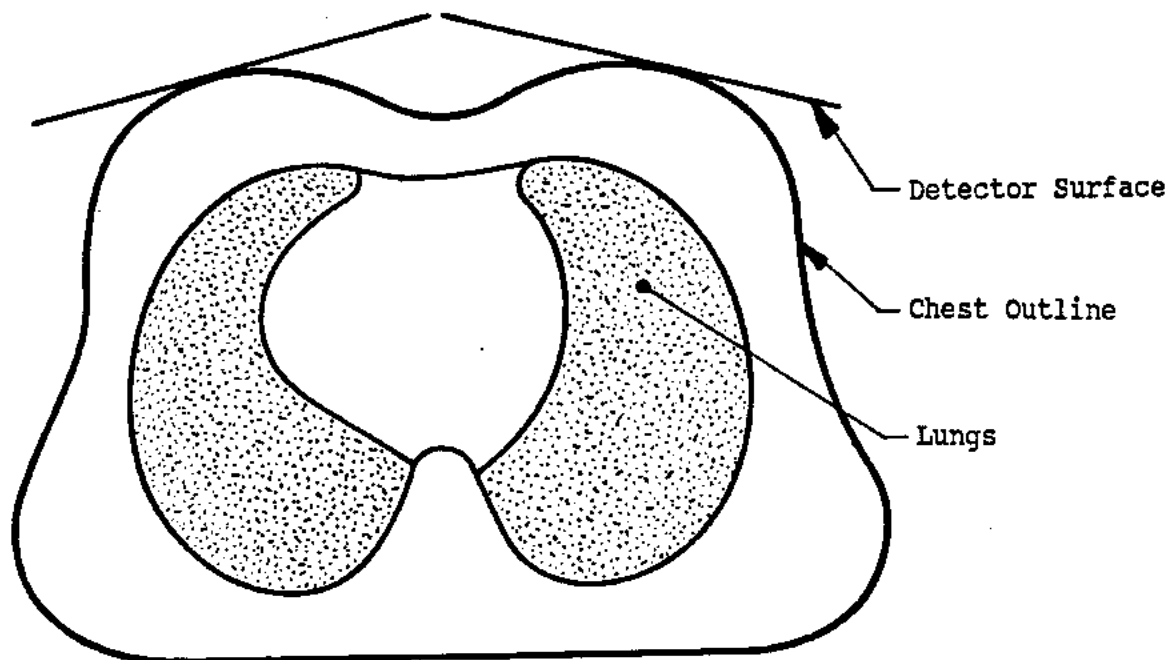
(b) Angled Across the Chest, AWRE Standard Geometry

FIGURE 2. COMPARISON OF THE TWO PAIRED 200 mm PHOSWICH DETECTOR GEOMETRIES
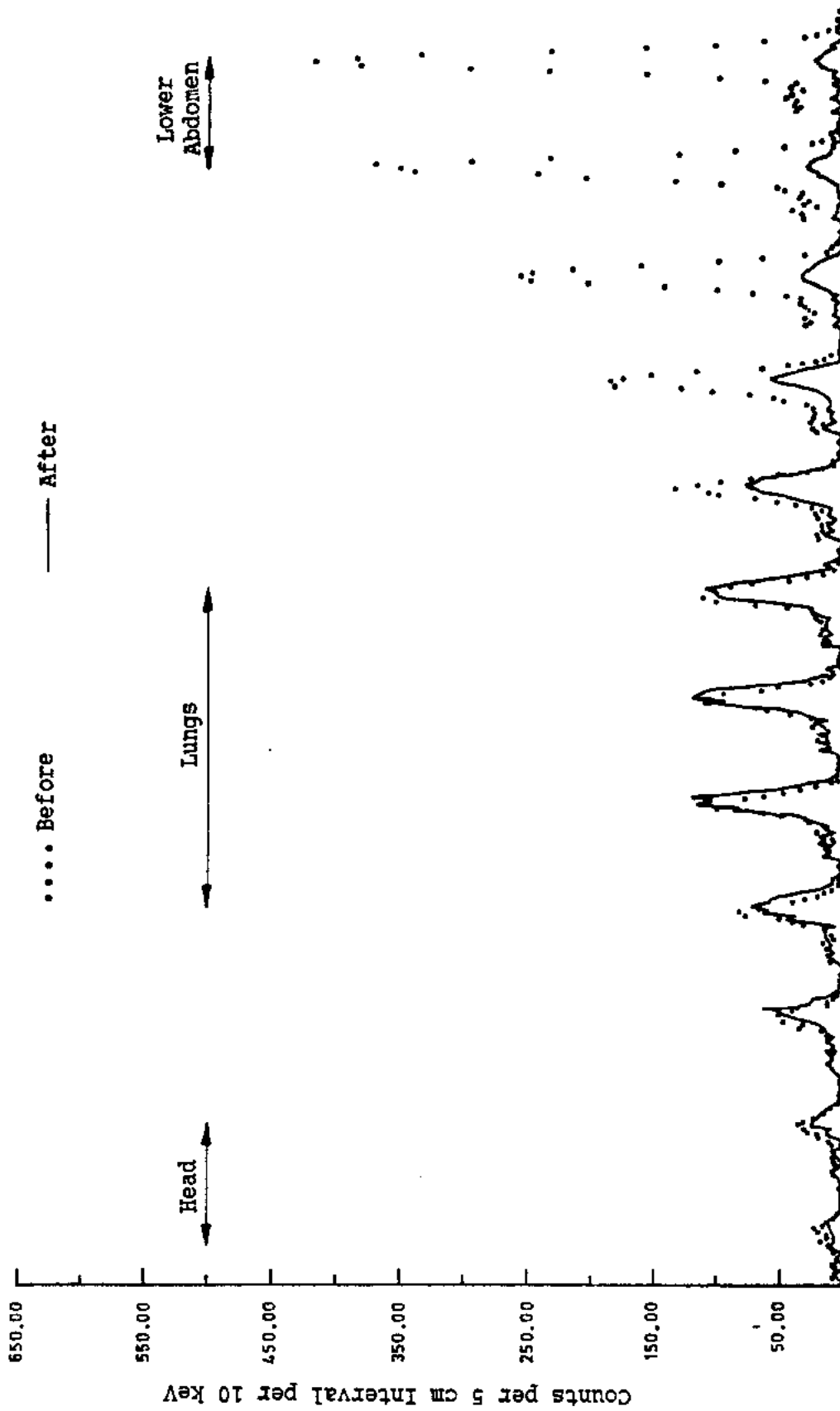
FIGURE 3. GAMMA SCANS, SUBJECT A, BEFORE AND AFTER GUT CLEARANCE USING A
COLLIMATED NaI(Tl) DETECTOR
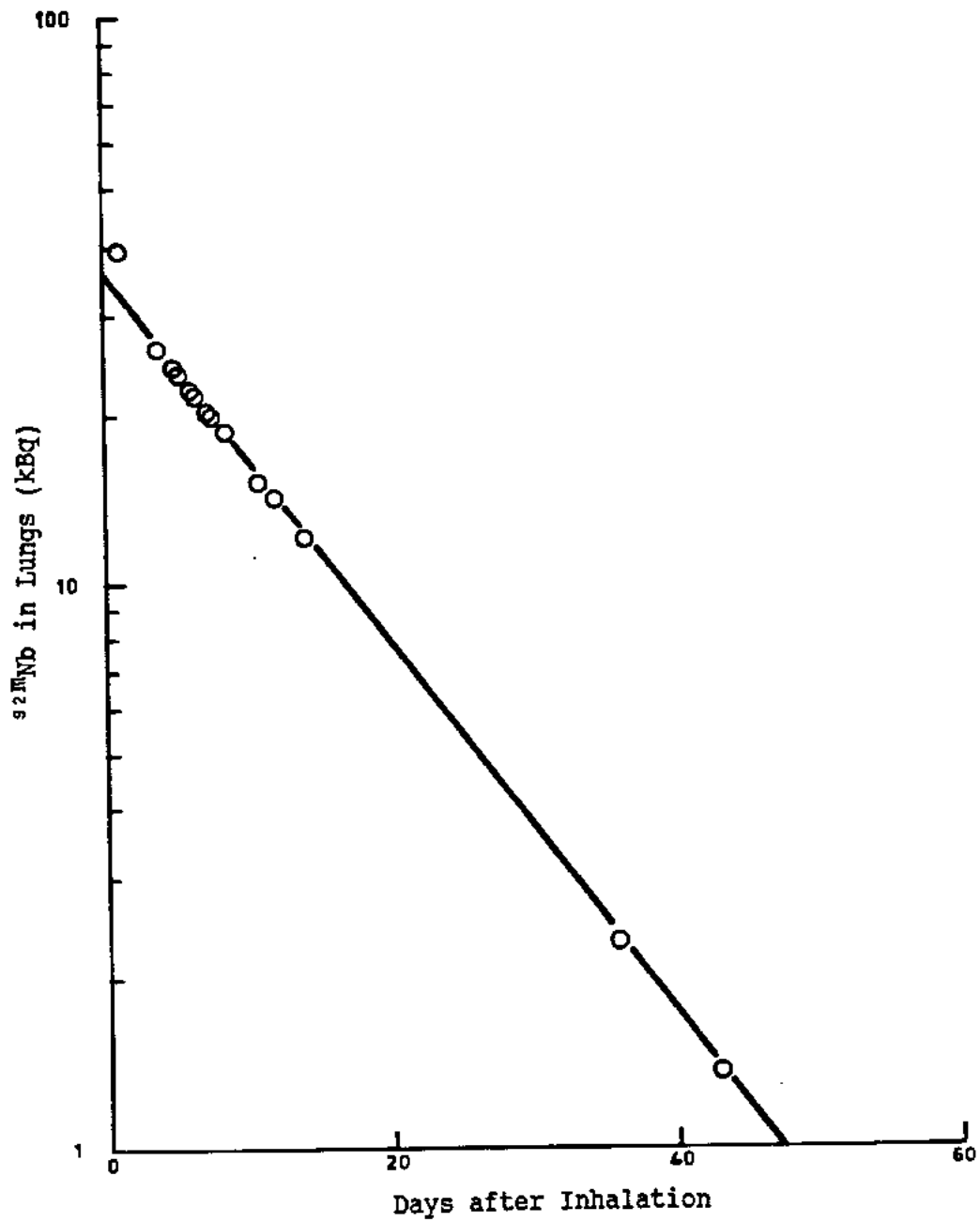
FIGURE 4. CLEARANCE OF ^{92m}Nb FROM THE LUNGS OF SUBJECT D FROM MEASUREMENTS
OF THE 934 keV GAMMA RAY EMISSIONS

FIGURE 4

35
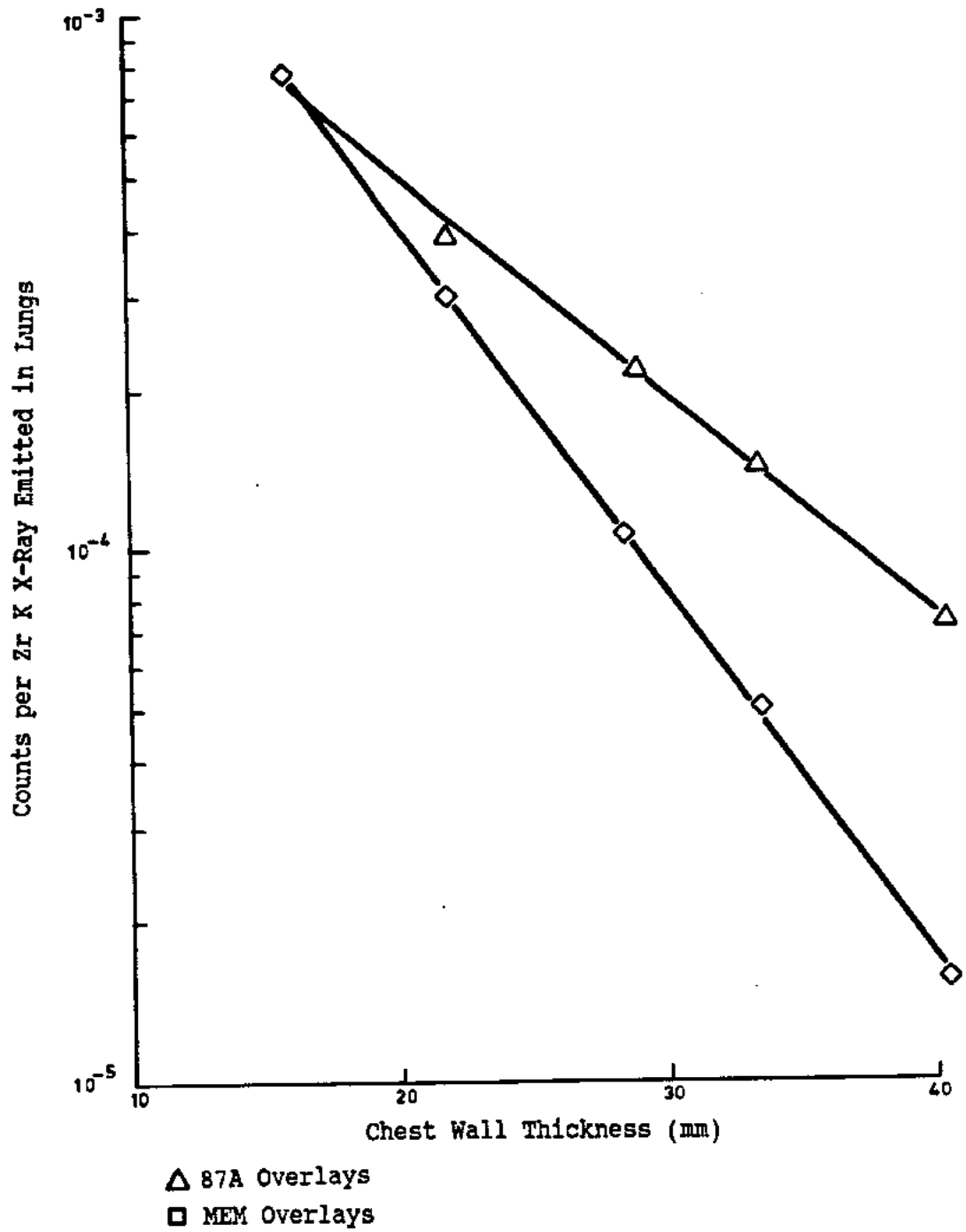
FIGURE 5. CALIBRATION CURVES FOR THE 200 mm DIAMETER PHOSWICH DETECTOR OVER THE RIGHT CHEST OF THE LLNL PHANTOM
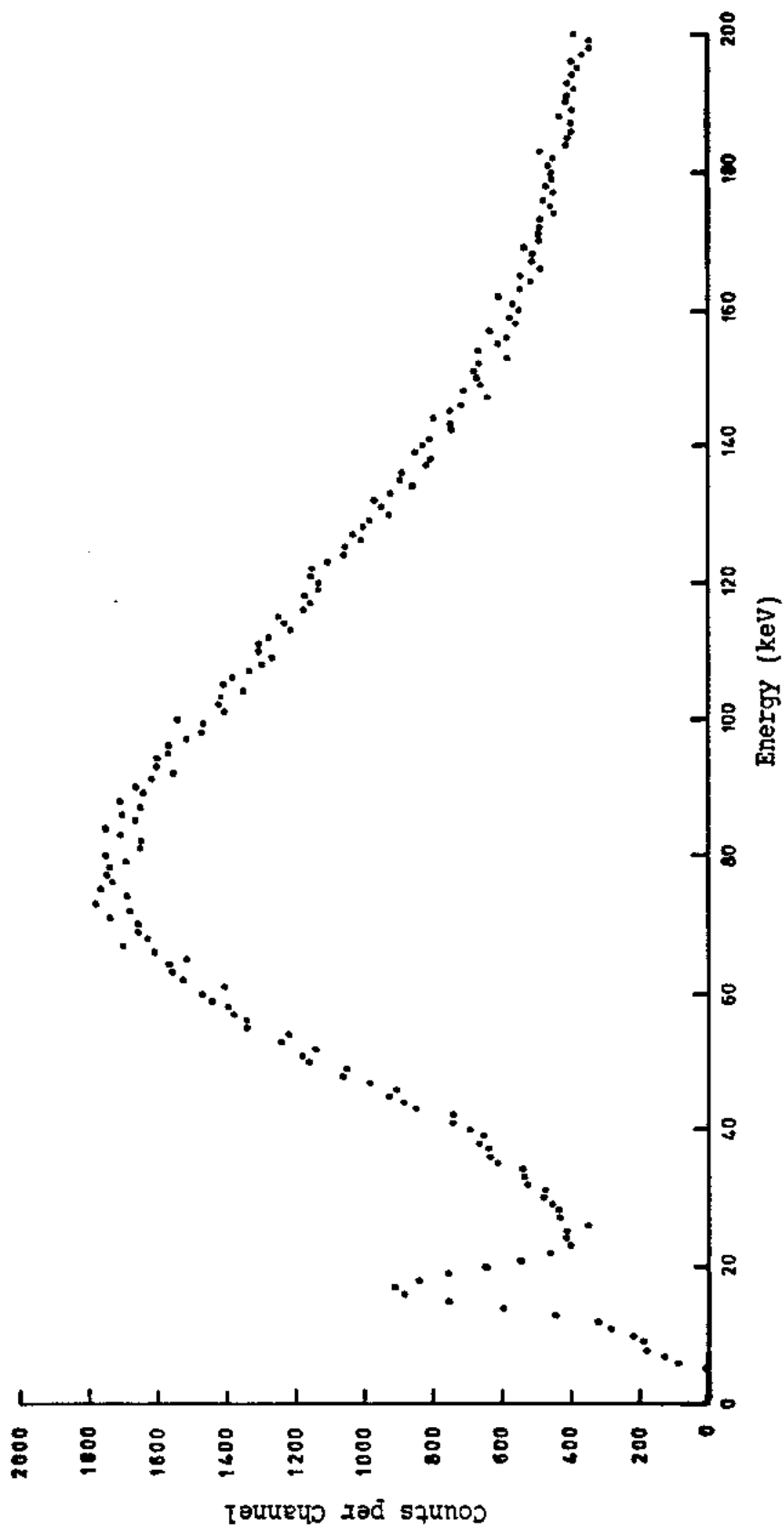
FIGURE 6. PHOSWICH SPECTRUM FROM SUBJECT D OBTAINED WITH A 200 mm DIAMETER
PHOSWICH DETECTOR IN THE CENTRAL GEOMETRY

37
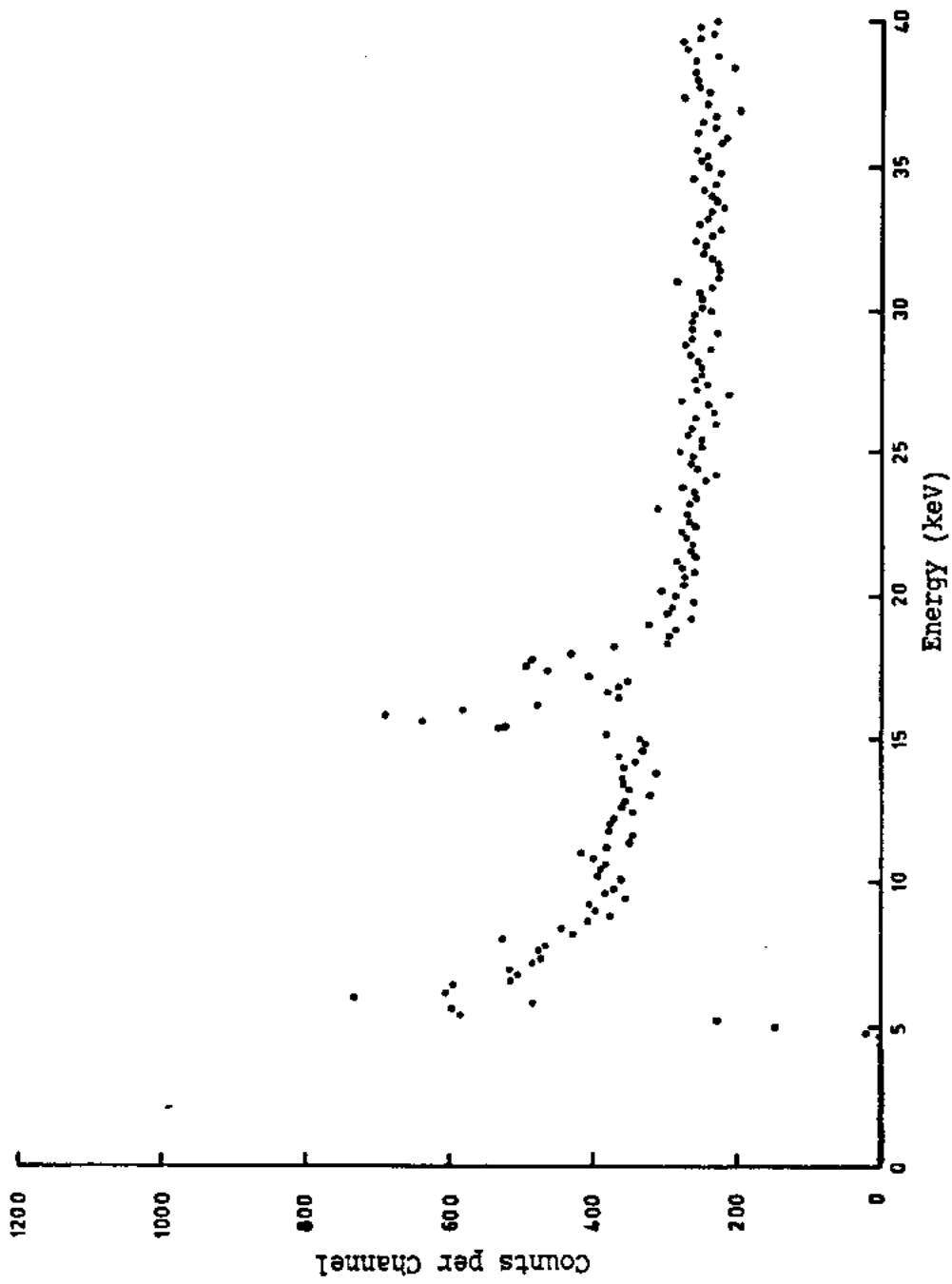
FIGURE 7. THE SUMMED GERMANIUM SPECTRUM FROM SUBJECT D OBTAINED WITH PAIRED
GERMANIUM ARRAYS
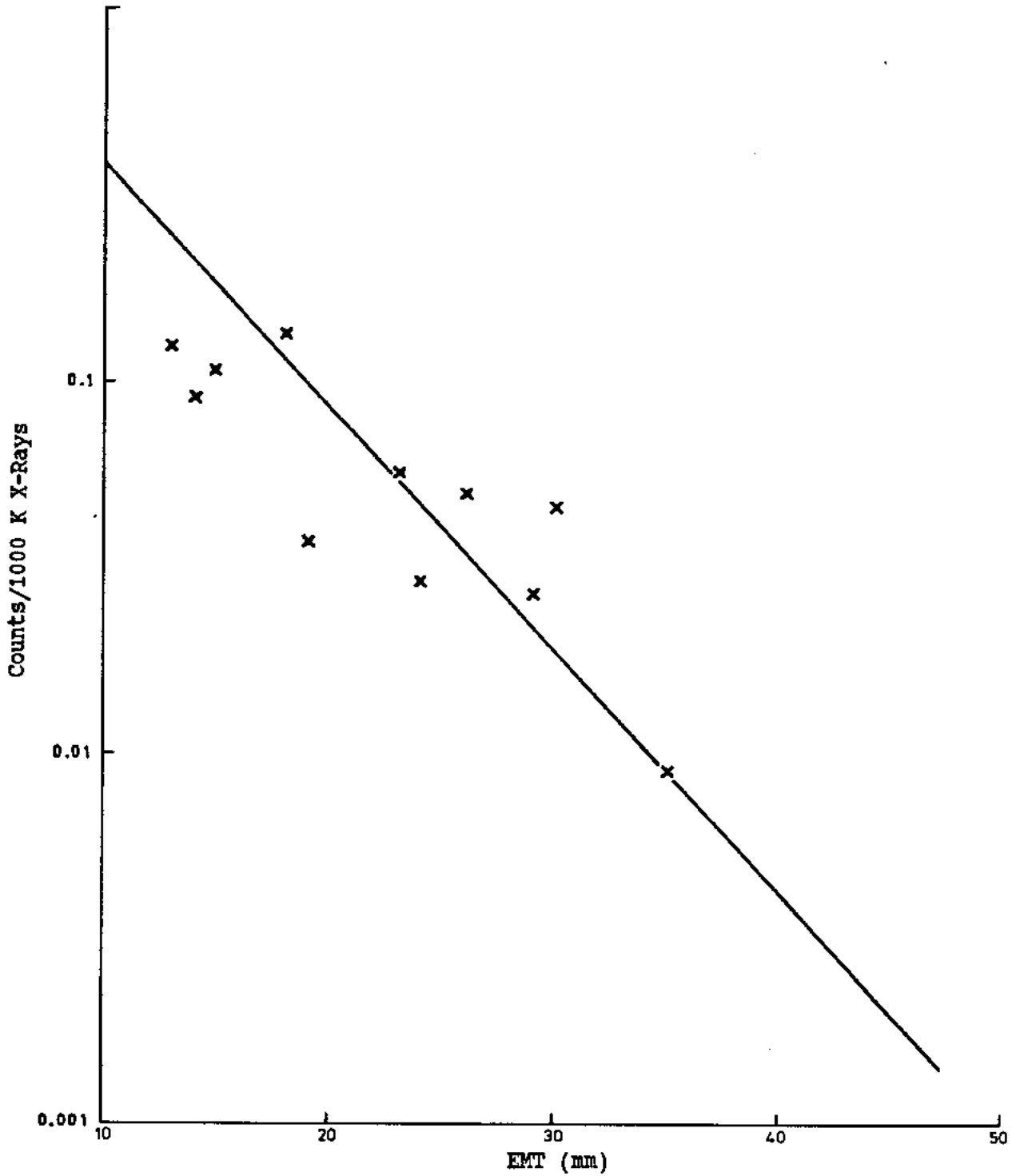
FIGURE 8. OBSERVED AND PREDICTED DETECTION EFFICIENCIES FOR THE CENTRAL GERMANIUM ARRAY GEOMETRY
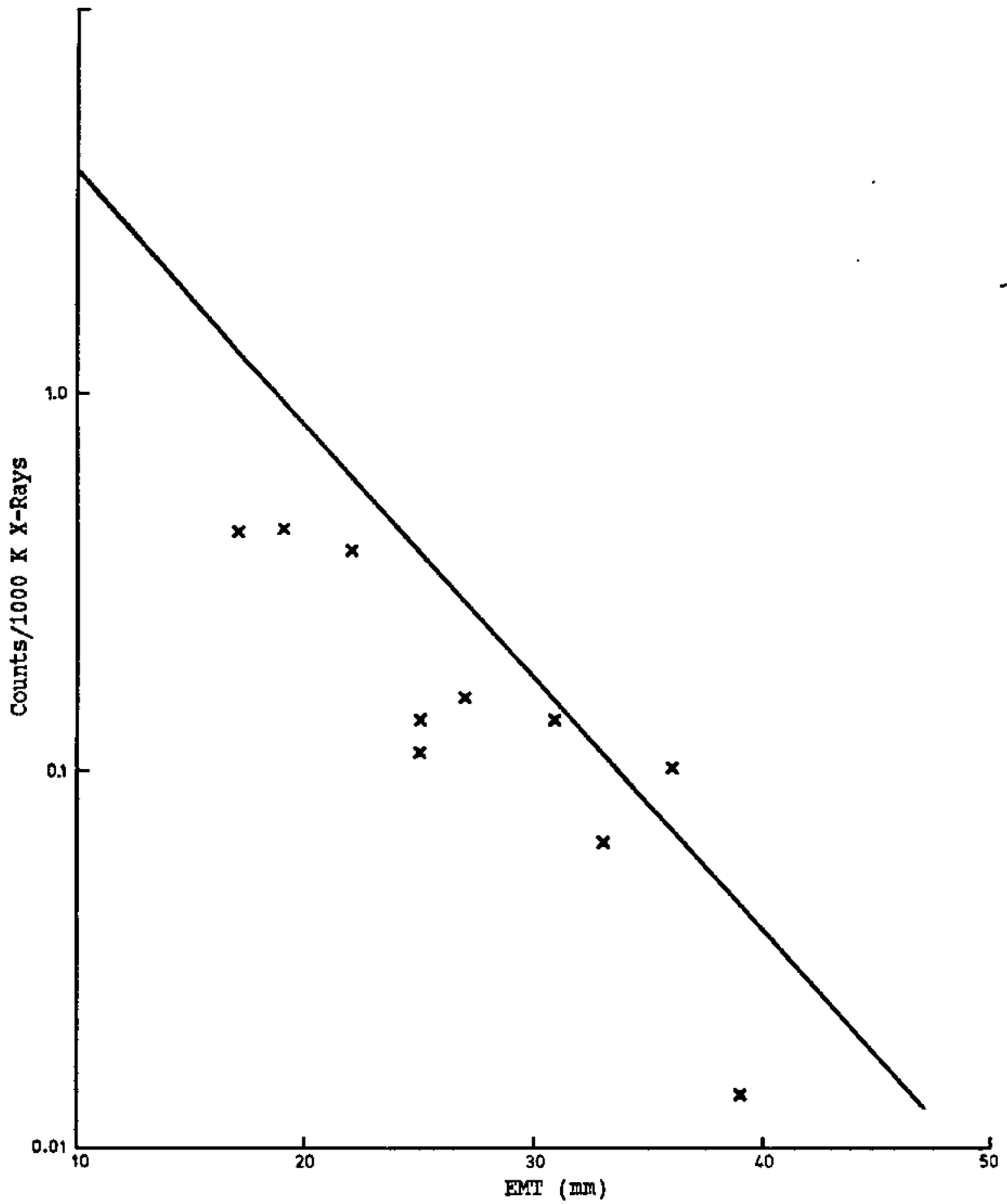
FIGURE 9. OBSERVED AND PREDICTED DETECTION EFFICIENCIES FOR THE DOUBLE
PHOSWICH GEOMETRY

AWRE O 24/87

ATOMIC WEAPONS RESEARCH ESTABLISHMENT

AWRE REPORT No. O 24/87

Investigation of the Distribution of Activity in the Lungs

and its Effect on the In-Vivo Measurement of Am-241
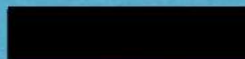
(UK UNCLASSIFIED)

This document is intended for publication in the open literature. Until it is published, it may not be circulated, abstracted or referred to outside the organisations to which copies have been sent.

AWRE,
MOD(PE),
Aldermaston, Berks.

June 1987

ATOMIC WEAPONS RESEARCH ESTABLISHMENT

AWRE REPORT NO. O 24/87

Investigation of the Distribution of Activity in the Lungs
and its Effect on the In-Vivo Measurement of Am-241
(UK UNCLASSIFIED)

Recommended for issue by

Approved by

CONTENTS

SUMMARY

The distribution of activity in the lungs following inhalation of
Nb-92m labelled polystyrene microspheres, has been investigated for two
female Caucasian subjects, using a collimated hyper-pure germanium
co-axial detector. Measurements of the 934 keV gamma-ray emissions from
the subjects' lungs have shown the distribution of activity to be
non-uniform.

Calibration measurements have been made with different source
distributions in the lungs of the Lawrence Livermore National Laboratory
(LLNL) anthropomorphic phantom. These suggest that when assessing Am-241
lung content with detectors positioned over the chest, errors of up to
300% can be introduced if a uniform distribution of activity in the lungs
is assumed.

1. INTRODUCTION

In a recent female intercalibration study, sponsored by the
IAEA*, the validity of using the LLNL male phantom (1) for calibrating
detectors used in the measurement of low energy X-ray emitters in the
lungs of women, was investigated (2). Eleven female volunteers with
various chestwall thicknesses and compositions inhaled Nb-92m labelled
polystyrene microspheres to compare measured detection efficiencies with
those predicted using the LLNL phantom. Calibration equations were
derived assuming the simplest case of uniform distribution of activity
within the lungs.

Nb-92m decays by electron capture with a half-life of 10.15 days,
emitting zirconium K X-rays at similar energies to the uranium L X-rays
from plutonium. A gamma ray photon is also emitted at an energy of 934
keV, which could be used to determine the lung content and hence the X-ray
emission rate, at any given time. An initial pulmonary deposit of up to
37 kBq allowed four to six weeks for X-ray measurements while keeping the
whole body dose equivalent to below 100 μSv.

Throughout the study, each volunteer spent a period of two weeks
at the AWRE Whole Body Monitoring Facility, where X-ray measurements were
made with either phoswich scintillation detectors or arrays of hyper-pure
germanium planar semi-conductor detectors. During such a period, two of
the volunteers were also monitored with an N-type germanium co-axial
detector, fitted with a simple collimator, to investigate the distribution
of inhaled Nb-92m labelled polystyrene microspheres within the lungs.

The results of these measurements prompted a further experiment
to assess the errors introduced on calibration with the LLNL phantom, when
assuming uniform distribution of activity within the lungs. An attempt
was made to mimic the observed distribution of activity, to see how it
might affect the calibration factors used in the routine analysis of
Am-241.

---

*Technical Contract 3362/TC

This report details the measurements made with the collimated hyper-pure germanium co-axial detector. A description of the calibration procedures using the LLNL phantom, is also given.

2.   DESCRIPTION OF SUBJECTS

The eleven female Caucasian subjects who participated in the female intercalibration study, were selected from healthy non-smoking volunteers to provide a range of ages, chestwall thicknesses and compositions. This selection process included measurement of the subject's chestwall using a Unirad, realtime, B-mode sonofluroscope, fitted with a 5 MHz transducer. The thickness and composition of the chestwall in the regions of interest, was therefore known for each subject.

Because priority was given to the low-energy X-ray measurements and due to the limited availability of detectors, the distribution of inhaled activity in the lungs was investigated for only two of the subjects. These were:-

3.   INHALATION OF AEROSOL

The Nb-92m was produced in the AERE Harwell variable energy cyclotron by alpha particle irradiation of yttrium. The activity was incorporated into a monodisperse aerosol of 3.5 μm polystyrene particles using previously developed methods (3).

The aerosol was then administered to each subject using an established technique (4). This involved inhaling the aerosol from a chamber by mouth, with the breathing pattern remaining natural and comfortable through the exposure.

After the irradiation each subject was monitored at the AERE Whole Body Monitoring Facility to determine the whole body Nb-92m content. If the total deposition was not sufficient to produce the initial pulmonary deposit required (18 to 37 kBq depending on chestwall thickness), a second "top-up" inhalation was arranged.

Subjects A and B inhaled the Nb-92m labelled polystyrene microspheres on the same day, giving initial pulmonary deposits of 30 kBq and 26 kBq respectively. However, it was decided that subject A, with a large chestwall thickness, should have a "top-up" inhalation, and this was conducted a week later.

4

Approximately three days after inhalation of the microspheres each subject was monitored at the AWRE Whole Body Monitoring Facility to determine whether gut clearance had been completed and activity remained only in the lungs (the microspheres which are deposited in the tracheo-bronchial region are removed by ciliary clearance up the trachea and into the gut from where they are excreted). A collimated NaI(Tl) detector was used to scan longitudinally over the upper part of the body to measure the distribution of activity. If gut clearance was incomplete the scan appeared asymmetric with increased counts towards the lower abdomen.

Once it was confirmed that gut clearance was completed (taking less than five days for each subject), measurements of the photon emissions from the subjects' lungs were started. For a number of subjects some measurements were possible before a "top-up" inhalation could be arranged. In the case of subject A this opportunity was taken to measure the distribution of activity in the lungs. Further measurements were subsequently made after the "top-up" inhalation to determine the new distribution of activity.

By comparison, subject B needed only one inhalation to produce the required initial pulmonary deposit. The distribution of activity in her lungs was therefore measured only once.

4.   DETECTOR CONFIGURATION

The N-type germanium co-axial detector used to determine the distribution of activity within the lung had a diameter of 54.7 mm and a depth of 54 mm, producing a detection volume of 126.9 cm^3. The germanium crystal was situated 3 mm behind a low background beryllium window of thickness 0.5 mm, and was fitted to a 1.21 Dewar flask with a static holding time of 24 h. The outer contact was ion-implanted to reduce low-energy X-ray spectral interference. A cylindrical copper collimator of length 13 cm, diameter 5.5 cm and thickness 4 cm was fitted over the detector, which was mounted on a moving platform. This allowed orientation of the detector and collimator arrangement in any direction. The intrinsic efficiency of the detector was measured to be 90% at 100 keV, falling to 18% at 1 MeV (5,6).

Spectral data were acquired with the detector connected via an Ortec 572 amplifier to an ADC in a nuclear Data Inc 6620 computer. The ADC was configured with 2048 channels of width 200 eV and the upper and lower gates were selected to give a recorded energy range of 800 keV to 1.21 MeV.

5.   DISTRIBUTION OF INHALED ACTIVITY

All measurements were made with the subject seated in a VDU operator's chair. A total of eight detector positions were investigated, with the detector viewing either the left or right lung. In each case the detector-collimator arrangement was orientated to maximise the surface area of contact with the chest. Positioning of the detector was achieved by using the clavicle, sternum and sternal notch as reference points. A count time of 20 min was selected for each detector position to minimise the discomfort to the subject, whilst still providing sufficient count data.

5.1 Measurements on subject A

5.1.1 Initial inhalation

Subject A was first monitored four days after her initial inhalation. Figure 1 represents the results of measurements made with the detector viewing the anterior and posterior chest. The numbers are the net counts observed in the 934 keV photopeak, for the particular detector geometry described by the circle.

Analysis of the count data for the anterior detector geometries show that the total net count recorded in the top two positions is a factor of (12 .8 ± 1.2)* greater than the total net count recorded in the bottom two positions. Since the 934 keV gamma rays are not significantly attenuated by the intervening tissue this results reflects a difference in the distribution of activity between the top and bottom of the lungs.

When monitoring the subject from the posterior aspect the number of counts recorded from each lung was similar to that recorded from the equivalent anterior detector position. This tends to confirm the view that the intervening tissue did not significantly attenuate the 934 keV gamma rays.

Lateral measurements of the subject's chest were also made, with the detector angled-in towards the armpits. The counts observed in the 934 keV photopeaks (shown in figure 2), were therefore due to emissions from the upper part of the lungs.

5.1.2 "Top-up" inhalation

The distribution of activity in the lungs was also measured six days after subject A's "top-up" inhalation (nine days after initial inhalation). Unfortunately, due to a shortage of time, only the anterior detector geometries could be investigated.

Figure 3 shows the net counts recorded in the 934 keV photopeak for each detector position. Analysis of the count data shows that the total net count recorded in the top two positions is a factor of (5.2 ± 0.4) greater than the total net count recorded in the bottom two positions. This again reflects a difference in the distribution of activity between the top and bottom of the lungs.

When comparing the observed counts with those recorded after the initial inhalation, it can be seen that the total net count recorded in the bottom two positions has increased by a factor of (2.1 ± 0.2). By comparison, the total net count recorded in the top two positions has decreased by a factor of (1.2 ± 0.05). However, no corrections have been made for the decay of the Nb-92m, or the clearance of the microspheres from the lungs after the first inhalation.

5.2 Measurements on subject B

Subject B was monitored four days following inhalation of the Nb-92m labelled polystyrene microspheres. Figure 4 shows the distribution of counts recorded with the detector viewing the anterior chest. Analysis

---

*All errors quoted at 95% confidence level

6

of the count data shows that the total net count recorded in the top two positions is a factor of (3.6 ± 0.2) greater than the total net count recorded in the bottom two positions. This again suggests a non-uniform distribution of activity in the lungs.

Lateral measurements of the subject's chest with the detector angled-in towards the armpit, gave the distribution of counts as shown in figure 5.

6.   CALIBRATION WITH LLNL ANTHROPOMORPHIC PHANTOM

At the AWRE Whole Body Monitoring Facility two arrays of hyper-pure germanium detectors have been used for the routine detection and measurement of uranium and the transuranic radionuclides in the chest, since 1982 (7). Each array consists of six planar hyperpure germanium semiconductor detectors of diameter 44 mm and effective thickness 7.5 mm, arranged in three rows of two in a rectangular vacuum containment box. The twelve detectors are separately connected to a Nuclear Data Inc 6620 computer, with ADC configured to give a recorded energy range of up to 204 keV. Thus twelve sets of detector pulse height spectra are independently acquired during routine operation.

The arrays are calibrated for in-vivo measurement of uranium and the transuranic radionuclides using the LLNL anthropomorphic phantom. Calibration measurements are made with the LLNL phantom containing lungs uniformly labelled with the isotope under investigation. Four overlays each with a 50% muscle, 50% adipose tissue content provide complete coverage of the phantom's anterior surfaces and allow simulation of chestwall thicknesses from 16 mm to 41 mm. Hence calibration equations relating the net count-rate per becquerel to the subject's chestwall thickness, are obtained for each isotope.

In order to assess the errors introduced on calibration with the LLNL phantom when assuming a uniform distribution of activity within the lungs, calibration data were obtained with two Amersham point sources attached to lungs which were uniformly labelled with 89 kBq Am-241. An attempt was made to mimic the distribution observed in the subjects by locating the Am-241 point sources in the upper contours of the lungs. Point sources of activity 425 and 434 kBq were taped to the left and right lungs respectively, giving a total lung content of 948 kBq Am-241. The distribution of activity was therefore in the ratio of approximately 10:1, biased towards the top of the lungs.

Two point source locations were investigated, as shown in figure 6. These were:-

(a) Position 1

The 434 kBq Am-241 source taped to the groove for the superior vena cava on the right lung and the 425 kBq Am-241 source taped in an equivalent position on the left lung. The sources were therefore approximately 20 cm from the anterior surfaces of the phantom's chestwall.

(b) Position 2

The 425 kBq Am-241 source taped to the groove for the aorta on the left lung and the 434 kBq Am-241 source taped in an equivalent position on the right lung. The sources were therefore approximately 26 cm from the anterior surfaces of the phantom's chestwall.

Calibration measurements were made using the same procedure as described above, with the arrays positioned in the standard geometry. Spectral data were acquired for a range of chestwall thicknesses to calibrate the arrays for the particular source arrangement (table 1). A least squares fit analysis was used to obtain the calibration equations.

The germanium arrays were therefore calibrated for a total of three source arrangements, including the uniform distribution of activity. Figure 7 shows a plot of the calibration data.

Analysis of the count data shows that when considering source position one the calibration factor, in terms of counts per minute per kilobecquerel Am-241, is approximately 30% larger than that for the uniform distribution. This means that the amount of Am-241 in the lungs could be over-estimated by 30% if the wrong source arrangement is assumed.

However, when considering the count data for source position two, the calibration factor is only a third of that for the uniform distribution. This result is rather more significant because it means that the amount of Am-241 in the lungs could be under-estimated by as much as 300%.

It is therefore clearly important to be cautious in the use of a calibration factor when assessing the amount of Am-241 in the lungs. In any case where a significant indication of contamination is observed evidence concerning the distribution of activity should be obtained. Large errors can be introduced by simply assuming that the activity is uniformly distributed throughout the lungs.

7. CONCLUDING REMARKS

It has been shown that when measuring the distribution of activity in the lungs following inhalation of Nb-92m labelled polystyrene microspheres, the majority of the activity appeared to be deposited in the upper regions of the lungs. The number of counts recorded from these regions was found to be up to a factor of (12.8 ± 1.2) greater than the counts recorded from the lower regions of the lungs. However, this factor was not constant and was observed to vary even for the same subject after a second inhalation.

A series of calibration measurements made with the LLNL anthropomorphic phantom containing lungs labelled with various distributions of Am-241, have shown that errors of up to 300% can be introduced if the wrong calibration factor is used. More information concerning the distribution of inhaled activity in the lungs is required before a confident estimate of lung content can be made from any measurement.

8. <u>ACKNOWLEDGEMENTS</u>

REFERENCES

1. R V Griffith, P N Dean, A L Anderson and J C Fisher: "A Tissue-Equivalent Torso Phantom for Intercalibration of an In-Vivo Transuranic Nuclide Counting Facility". Advances in Radiation Protection Monitoring, 493-503, IAEA Vienna (1979)

2. ██████████████████████: "Calibration of X-ray Counters for Assessment of Internal Lung Contamination, with Low Energy X-ray Emitters, in Women. Part 1: Measurements Made at AWRE Aldermaston". AWRE Report No. O 7/86

3. R G Fleming: "The Production of Niobium-92 Labelled 5 μm Diameter Polystyrene Microspheres". AERE-R 670, HMSO (1980)

4. M Walsh, A Black and N Foord: "Apparatus for the Administration by Inhalation of Radioactive Particles to Human Subjects for Studies of Deposition and Clearance". J Aerosol Sci. <u>8</u>, 83-90 (1977)

5. ██████████████████████: "The Evaluation of Three Commercially Available High-Purity Germanium Photon Spectrometers, for In-Vivo Measurement of Uranium and Transuranic Radionuclides". AWRE Report No. O 20/86

6. ████████: Private Communication, 1986

7. R C Lane, W B McCormick, S J Jefferies and P Danyluk: "Use of Six-Element Arrays of Hyperpure Germanium Detectors in Monitoring for Internal Actinide Contamination". Assessment of Radioactive Contamination in Man, 1984, 77-92, IAEA Vienna (1985)

TABLE 1

Calibration Data for Germanium Arrays

Source Arrangement	Chestwall Thickness (mm)	Counts/min/kBq Am-241
Position 1		
	16.0	226
	22.0	184
	28.5	157
	33.5	135
	41.0	108
Position 2		
	16.0	60
	22.0	48
	28.5	40
	33.5	33
	41.0	28
Uniform		
	16.0	176
	22.0	144
	28.5	119
	33.5	102
	41.0	81

Calibration equations

Position 1 $cpm/kBq = 356 \exp(-0.0290 \ CWT)$

Position 2 $cpm/kBq = 98 \exp(-0.0313 \ CWT)$

Uniform $cpm/kBq = 285 \exp(-0.0307 \ CWT)$
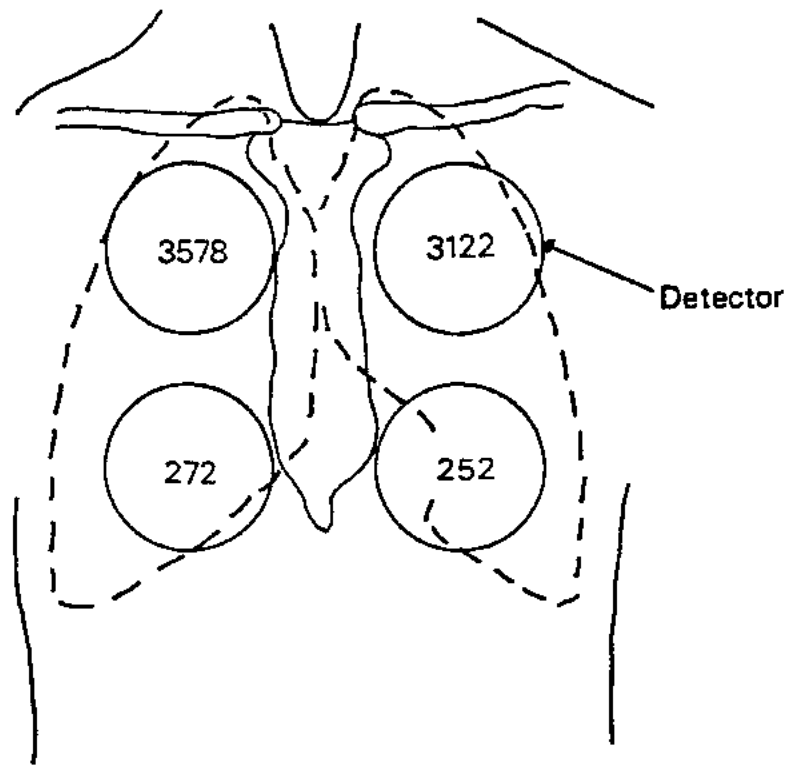
Anterior View
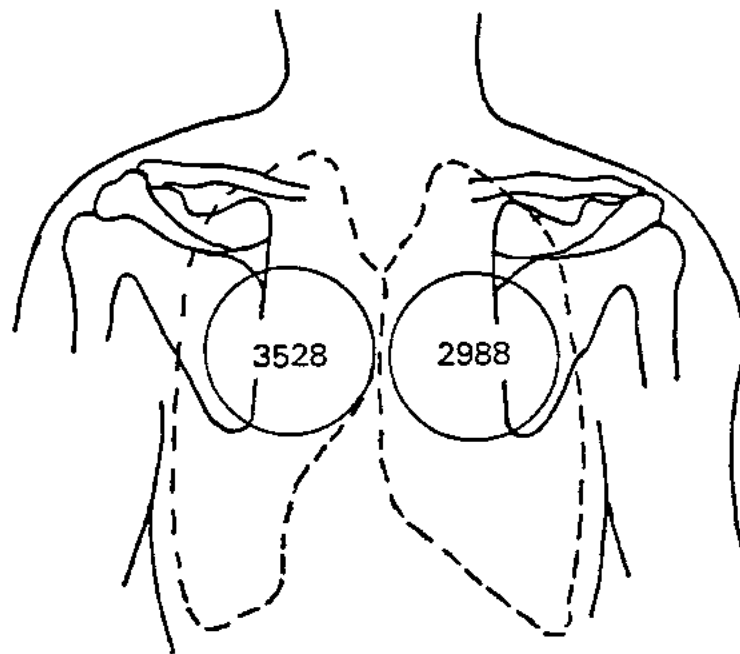
Posterior View

FIGURE 1. ANTERIOR AND POSTERIOR MEASUREMENT OF SUBJECT A

Left Lateral View

2113

Detector

3075

Right Lateral View
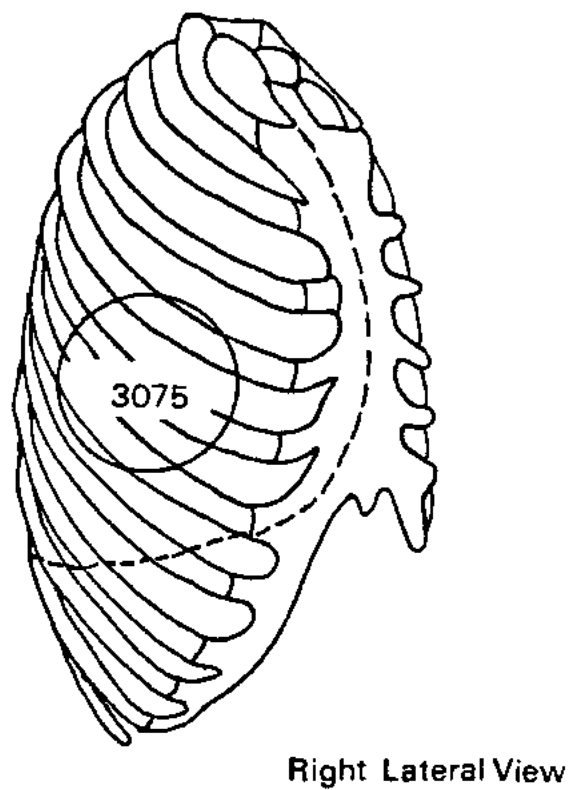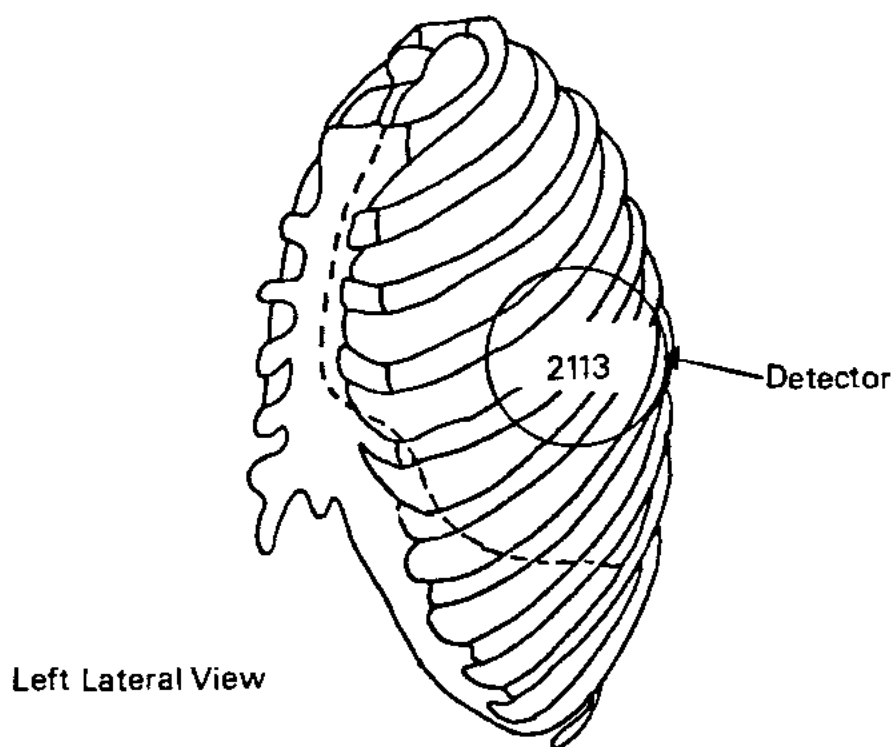
FIGURE 2. LATERAL MEASUREMENT OF SUBJECT A

12
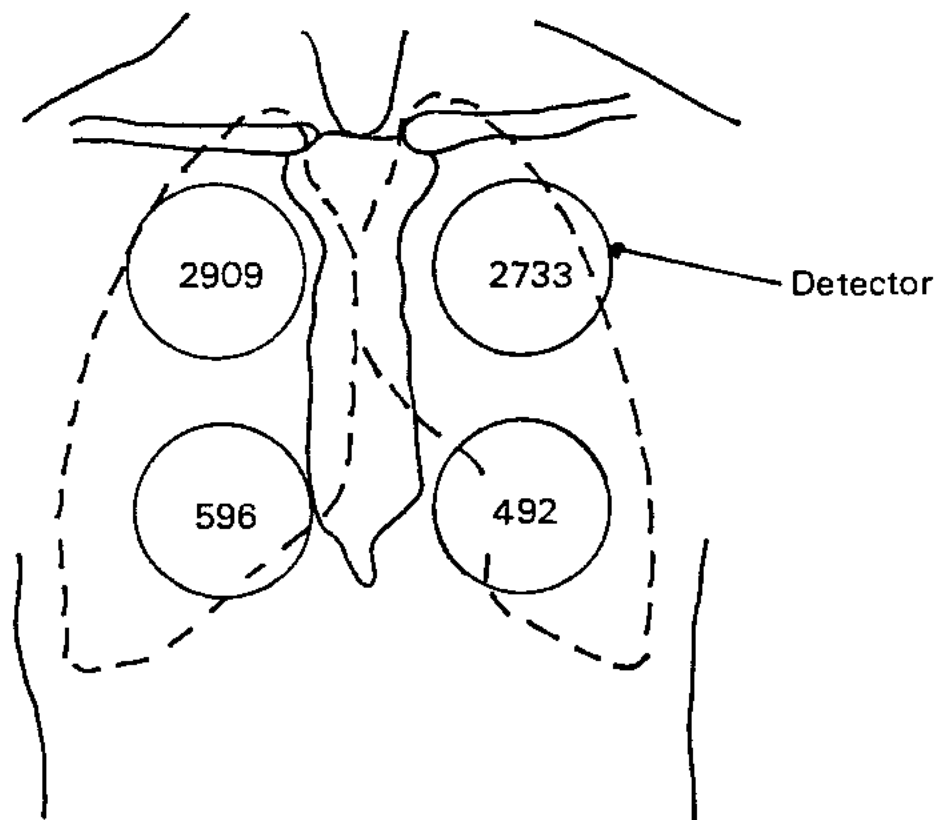
Anterior View

FIGURE 3. ANTERIOR MEASUREMENT OF SUBJECT A

13
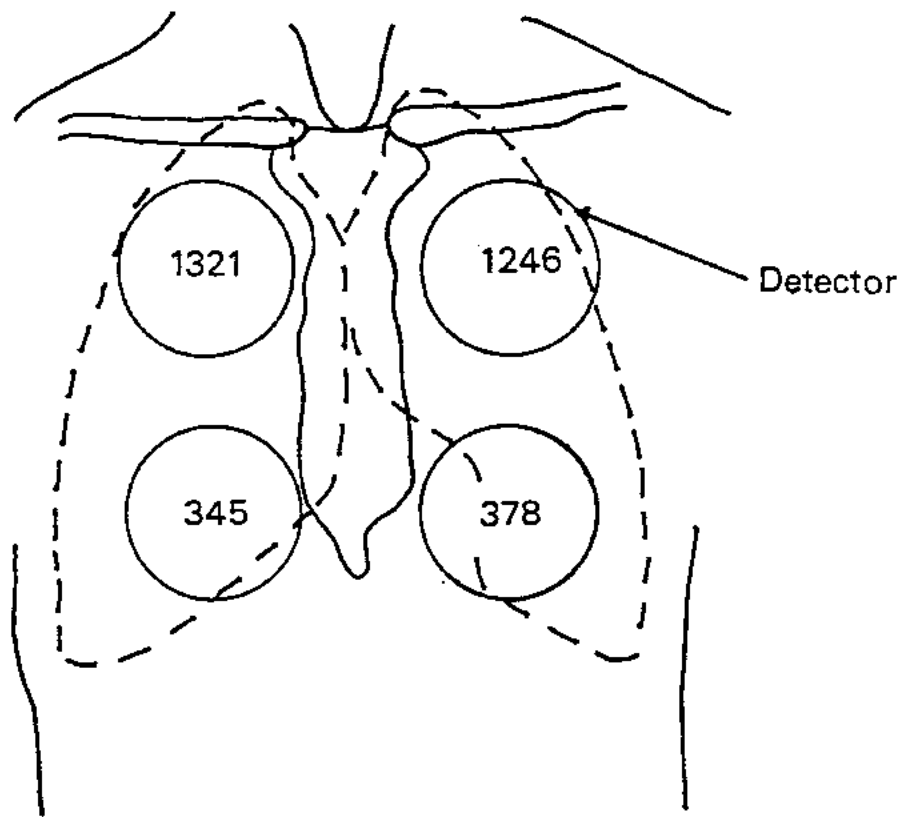
Anterior View

FIGURE 4. ANTERIOR MEASUREMENT OF SUBJECT B
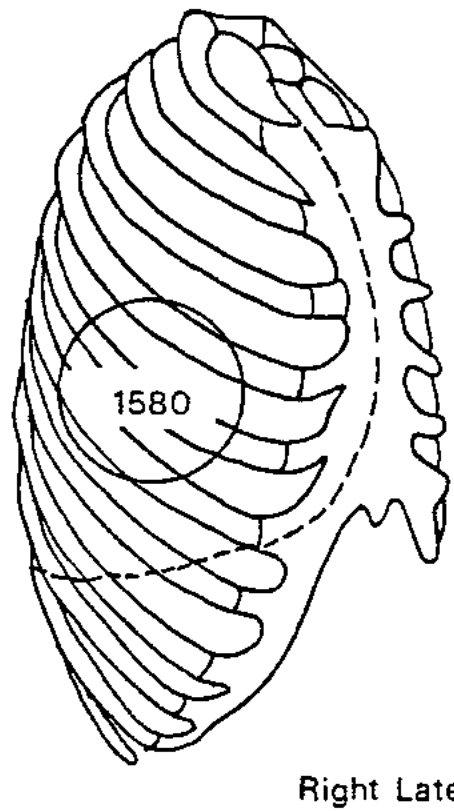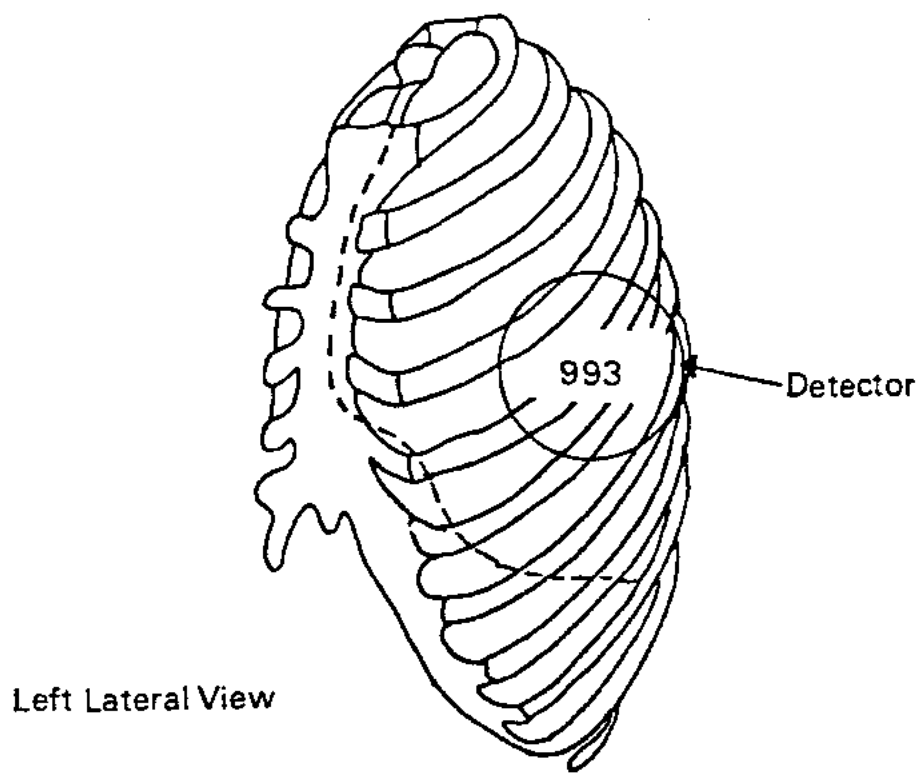
14

Left Lateral View

993 —Detector

Right Lateral View

1580

FIGURE 5. LATERAL MEASUREMENT OF SUBJECT B

15

Groove for Aorta

LEFT LUNG

Anterior Border

Groove for Superior Vena Cava

RIGHT LUNG

Anterior Border
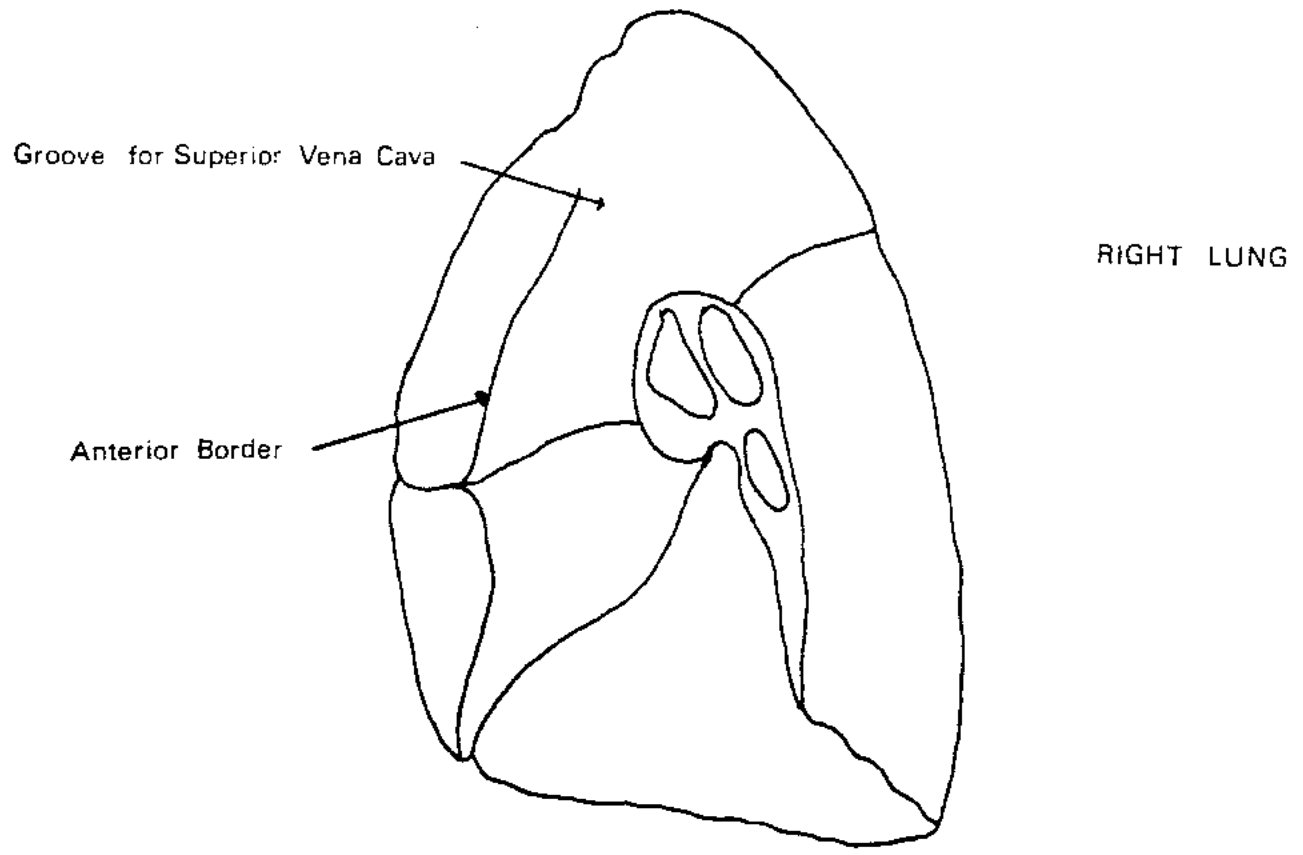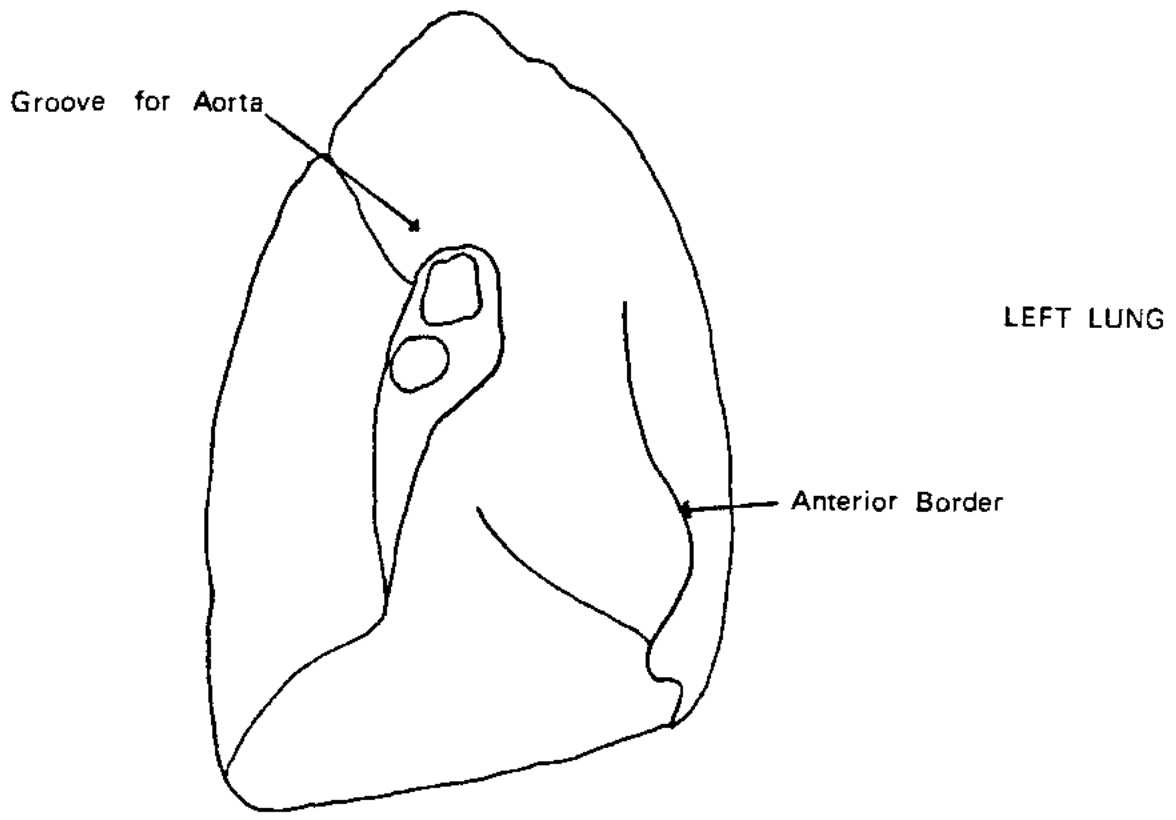
FIGURE 6. POSITIONING OF Am-241 POINT SOURCES ON THE MEDIAL SURFACES
OF THE LUNGS

16
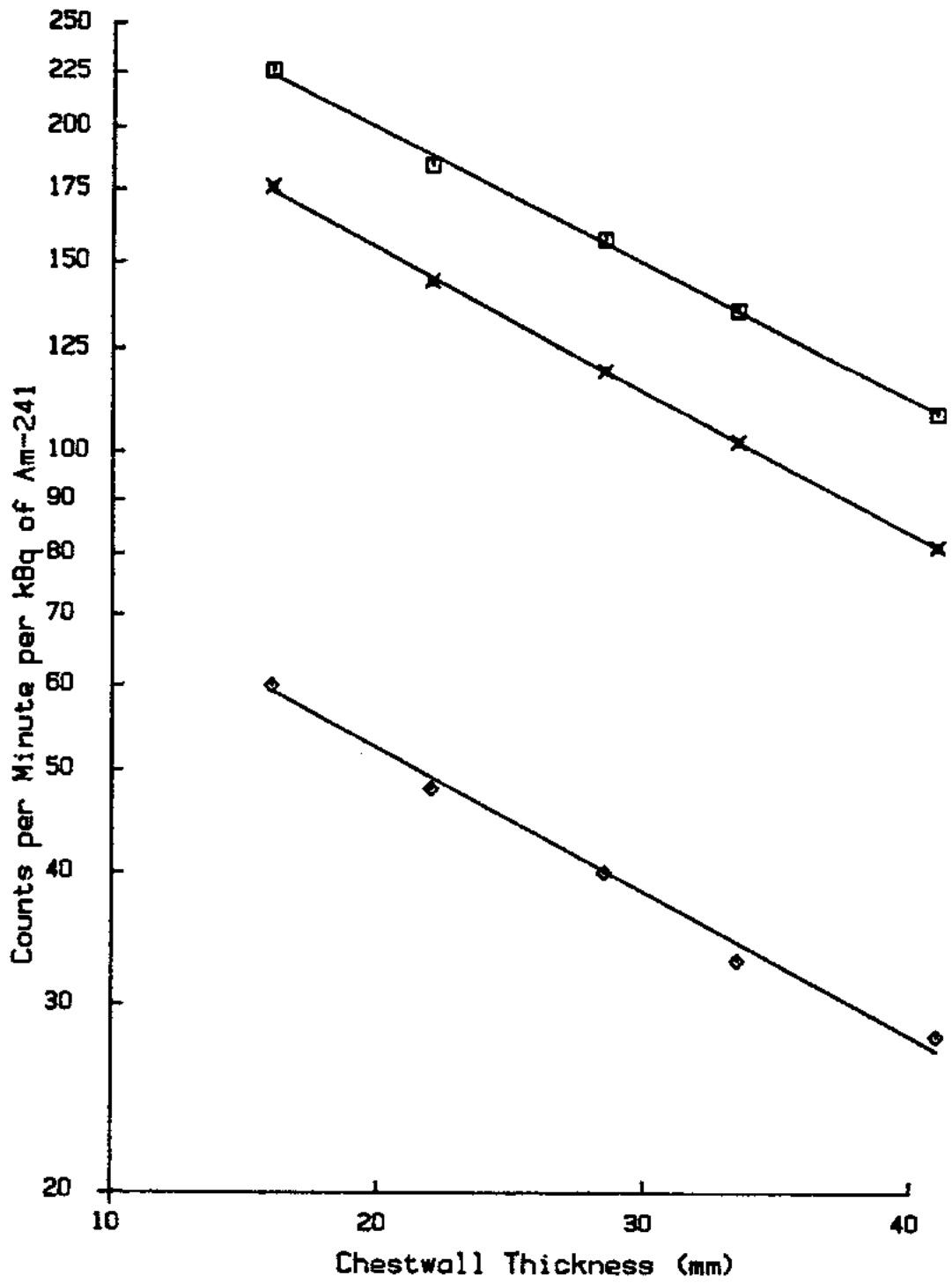
FIGURE 7. CALIBRATION OF GERMANIUM ARRAYS